Notch signaling represses cone photoreceptor formation through the regulation of retinal progenitor cell states

Xueqing Chen[1,2], Mark M. Emerson[1,2,3*]

[1] Biology PhD Program, The Graduate Center, The City University of New York, New York, NY, 10016

[2] Department of Biology, The City College of New York, The City University of New York, New York, NY, 10031

[3] Biochemistry PhD Program, The Graduate Center, The City University of New York, New York, NY, 10016

*Corresponding author: memerson@ccny.cuny.edu

Email addresses:

Xueqing Chen: xchen2@gradcenter.cuny.edu

Mark Emerson: memerson@ccny.cuny.edu

Keywords: retinal progenitor cells, multipotency, cis-regulation, cone photoreceptors, Notch inhibition, dominant-negative, chicken, electroporation

Abstract

Notch signaling is required to repress the formation of vertebrate cone photoreceptors and to maintain the proliferative potential of multipotent retinal progenitor cells. However, the mechanism by which Notch signaling controls these processes is unknown. Recently, restricted retinal progenitor cells with limited proliferation capacity and that preferentially generate cone photoreceptors have been identified. Thus, there are several potential steps during cone genesis that Notch signaling could act. Here we use cell type specific cis-regulatory elements to localize the primary role of Notch signaling in cone genesis to the formation of restricted retinal progenitor cells from multipotent retinal progenitor cells. Localized inhibition of Notch signaling in restricted progenitor cells does not alter the number of cones derived from these cells. Cell cycle promotion is not a primary effect of Notch signaling but an indirect effect on progenitor cell state transitions that leads to depletion of the multipotent progenitor cell population. Taken together, this suggests that the role of Notch signaling in cone photoreceptor formation and proliferation are both mediated by a localized function of Notch in multipotent retinal progenitor cells to repress the formation of restricted progenitor cells.

Introduction

Notch signaling is an evolutionarily conserved signaling pathway that functions in diverse cellular contexts to drive both cell cycle and cell fate decisions. In canonical Notch signaling, extracellular binding of a member of the Delta/Serrate/Lag family of proteins to the extracellular portion of the transmembrane Notch receptor leads to a proteolytic cleavage that releases the Notch intracellular domain (NICD) from the membrane (Bray, 2006; Kopan and Ilagan, 2009). The NICD then translocates to the nucleus, and through a primary interaction with the MAML protein, forms a tripartite complex with the Rbpj transcription factor that affects transcription of target genes (Mumm and Kopan, 2000; Wu et al., 2000). Notch signaling can act iteratively and

participate in several distinct decisions that occur during the process of formation of a particular cell type. For example, during the formation of Drosophila sensory neurons from ectoderm, Notch signaling is critical in three successive cell fate decisions (Artavanis-Tsakonas et al., 1991; Bray, 1998).

During the formation of the vertebrate retina, a functional role for Notch signaling in both proliferation and in cell fate choice has been identified (Hayes et al., 2007; Henrique et al., 1997; Jadhav et al., 2006a; Mizeracka et al., 2013a; Nelson et al., 2007). Induction of conditional loss-of-function alleles for the Notch1 receptor during early retinogenesis leads to cell cycle exit and increased cone photoreceptor formation (Jadhav et al., 2006b; Yaron et al., 2006). In one of these studies, a loss of horizontal cells (HCs) was also described (Yaron et al., 2006). Similarly, conditional Rbpj loss-of-function increases the formation of cone photoreceptors while also promoting the formation of retinal ganglion cells (RGCs) (Riesenberg et al., 2009). Both Notch1 and Rbpj loss-of-function conditions result in decreased proliferation. Conditional loss of Notch1 in the later postnatal period, after the window of cone genesis, reveals that rod photoreceptors are also increased, which suggests that Notch signaling plays a more general role in repression of the photoreceptor fate (Jadhav et al., 2006b). In addition, it has been suggested in this postnatal context that Notch signaling can function in postmitotic cell fates to repress the rod fate (Mizeracka et al., 2013b).

While a role for Notch signaling in the generation of cone photoreceptors has been identified, the pan-retinal inhibition of Notch signaling through chemical inhibition and conditional alleles has not allowed for a specific role of Notch to be determined. Recently, the formation of cones has been identified as a multistep process. During the early stages of retinal formation when cone photoreceptors are preferentially generated, multipotent retinal progenitor cells (RPCs) divide to form restricted (also known as neurogenic RPCs) RPCs that can be identified by the activity of Thrb cis-regulatory elements, the expression of specific transcription factors (Otx2, OC1 and Olig2), and the

91 decreased expression of canonical RPC markers, such as Vsx2
92 (Buenaventura et al., 2018; Emerson and Cepko, 2011; Emerson et al., 2013;
93 Hafler et al., 2012; Jean-Charles et al., 2018; Suzuki et al., 2013). These
94 restricted RPCs lack the diverse cell fate potential of multipotent RPCs, and
95 instead, preferentially divide to form cone and HCs as well as a minor number
96 of RGCs (Cepko, 2014; Emerson et al., 2013; Schick et al., 2019). Thus,
97 Notch signaling could mediate cone genesis through regulation of the
98 multipotent to restricted RPC transition, the cell fate choices of the restricted
99 RPC daughter cells, or in the production of cones directly from multipotent
100 RPCs or other cell types.
101 In this study, we used defined cis-regulatory elements to both quantitate
102 the effects of Notch signaling inhibition and also to limit interference with
103 Notch signaling to specific cell types. We determined that during the formation
104 of cone photoreceptors, inhibition of Notch signaling specifically promoted the
105 formation of restricted RPCs from multipotent RPCs but did not promote the
106 cone fate in the daughter cells of restricted RPCs. As expected for such a shift
107 in cycling populations, there was minimal short-term effect on proliferation as
108 measured by EdU labeling. Taken together, this suggests that a primary role
109 of Notch signaling during cone photoreceptor genesis is to regulate the
110 formation of restricted RPC states from multipotent RPCs.
111

112 **Results**

113 **Evaluation of Notch reporter activity in response to MAML dominant-**
114 **negative**

115 To provide cell-type specific precision and rapid interference with Notch
116 signaling, we used a dominant-negative approach. We first created a chicken
117 version of a previously validated, and widely used, C-terminal truncation
118 version of MAML that retains the ability to interact with the Notch intracellular
119 domain but lacks the domains necessary to induce a transcriptional response
120 (referred to as MAML-DN) (Tan et al., 2016; Weng et al., 2003). The chicken

121 MAML1 gene was used, as it was the MAML gene most highly expressed in
122 the developing chicken retina according to reported RNA-Seq data
123 (Buenaventura et al., 2018). The reported MAML-DN construct encoded a
124 fusion protein with the N-terminal region of MAML placed N-terminal to GFP.
125 However, we expected to use GFP reporters as an output in our experiments,
126 and so engineered a fusion protein of the MAML N-terminal region with
127 GAPDH instead of GFP. Two AU1 tags were added to aid in tracking the
128 expression of the protein (Fig 1A) (Shevtsova et al., 2006).
129 To test the effectiveness of the MAML-DN construct, we used a
130 previously validated chicken Notch reporter - Hes5::GFP (Vilas-Boas et al.,
131 2011). This reporter uses both transcriptional regulatory elements and 3'
132 untranslated regions of the chicken Hes5-1 gene, which was previously
133 identified as a target of Notch signaling during chicken development (Fior and
134 Henrique, 2005).
135 E5 chicken retinas were co-electroporated ex vivo with Hes5::GFP, a
136 ubiquitous electroporation control (CAG::Nucßgal), and with or without the
137 MAML-DN construct. After two days of culture, retinas were imaged by
138 confocal microscopy or analyzed by flow cytometry (Fig. 1A). In control
139 retinas, the Hes5::GFP reporter was active primarily in the neuroblast layer of
140 the retina, where multipotent RPCs are located, and the reporter activity was
141 drastically abrogated in response to MAML-DN introduction (Fig. 1B).
142 Strikingly, we found in all the experimental groups that the retinal distribution
143 of the electroporated population was altered, with cells found predominantly in
144 the scleral region where photoreceptor cells and Otx2/OC1+ RPCs are
145 enriched, as well as the RGC layer, but not in the middle portion of the retina
146 where most multipotent RPCs are localized (Fig. 1B) (Buenaventura et al.,
147 2018). To test the specificity of the effects observed with this MAML-DN
148 construct, a plasmid encoding an AU1-GAPDH protein without the MAML N-
149 terminal region was used in the same experimental workflow. A typical
150 distribution of cells and levels of the Hes5::GFP reporter were observed with

151 this control construct (Fig. S1A). Immunofluorescent detection of the AU1 tag
152 revealed a predominantly cytoplasmic distribution for the AU1-GAPDH
153 construct that appeared more nuclear in the MAML-DN version (Fig. S1A).
154 To quantify Notch reporter activity, we used a flow cytometry assay and
155 calculated the percentage of GFP-positive cells within the electroporated cell
156 population (Fig. 1C). The quantification supported the conclusions of the
157 confocal imaging results, as Hes5::GFP reporter activity showed a significant
158 decrease in response to MAML-DN introduction. The negative control AU1-
159 GAPDH vector did not interfere with the Hes5::GFP activity (Fig. S1B). To
160 further confirm this effect, we employed an alternative dominant-negative
161 strategy in which we N-terminally or C-terminally fused the repressor domain
162 of engrailed to the full-length Rbpj protein coding sequence (EnR-Rbpj or
163 Rbpj-EnR). This modification would be predicted to convert Rbpj into a
164 dedicated repressor that would continually repress Notch target genes, even
165 under conditions of active Notch signaling (Vickers and Sharrocks, 2002). In
166 addition, we created a plasmid that would express a Rbpj protein with a
167 R218H mutation, which was previously characterized as a dominant-negative
168 form of Rbpj (Chung et al., 1994). Hes5 reporter activity was significantly
169 decreased in the presence of all four dominant-negative constructs, thus
170 identifying multiple dominant-negative approaches to inhibit Notch signaling
171 (Fig. 1 and Fig. S2).
172
173 **Inhibition of Notch promotes the formation of restricted progenitor cells**
174 A mouse knockout of the Notch1 receptor leads to an increase in cone
175 photoreceptors (Jadhav et al., 2006b; Yaron et al., 2006), but the mechanism
176 behind this phenotype is unknown. One possibility is that in the knockout,
177 multipotent RPCs produce more of the RPC type that is restricted to cone and
178 HC fates, which in turn divide to form cones. The cis-regulatory element
179 ThrbCRM1 provides a robust tool to answer the question as it is active
180 specifically in this restricted RPC type (Emerson et al., 2013).

181 We first tested the effect of Notch inhibition on specific cell types using
182 DNA reporters, including reporters with enrichment in multipotent RPCs
183 (VSX2ECR4; Buenaventura et al., 2018), cone/HC restricted RPCs
184 (ThrbCRM1; Emerson et al., 2013), subsets of cones (ThrbCRM2; Emerson et
185 al., 2013; Schick et al., 2019) and HCs/RGCs (OC1ECR22; Patoori et al.,
186 2020; Schick et al., 2020). E5 chicken retinas were co-electroporated with an
187 electroporation control, with or without the MAML-DN, and assessed by
188 confocal microscopy after two days culture. In retinas in which MAML-DN was
189 introduced, the number of ThrbCRM1 reporter-labeled restricted RPCs was
190 visibly increased, while the number of VSX2ECR4-labeled multipotent RPCs
191 was decreased and presented with altered morphology (Fig. 2A). The number
192 of ThrbCRM2 reporter-labeled cones and OC1ECR22 reporter-labeled
193 HCs/RGCs were qualitatively unchanged at this timepoint (Fig. S3A). The
194 quantification of these cell types using flow cytometry statistically confirmed
195 these effects (Fig. 2B). In addition, in retinas in which VSX2ECR4::GFP and
196 ThrbCRM1::TdTomato were co-electroporated, the number of GFP/TdTomato
197 double-positive cells dramatically increased from the low amount that is
198 typically observed (Buenaventura et al., 2018). Taken together, this suggests
199 that the broad inhibition of Notch signaling leads to the formation of
200 supernumerary ThrbCRM1 cells and these new cells are derived from
201 multipotent RPCs. To confirm the specificity of the MAML-DN effect on
202 ThrbCRM1, we used the AU1-GAPDH as a negative control and observed no
203 significant change in ThrbCRM1::GFP levels (Fig. S1B). Intriguingly,
204 ThrbCRM2-labeled cones did not significantly increase after 2 days culture,
205 which could indicate a delay in cone genesis at this time point.
206 The increase in ThrbCRM1 reporter-positive cells could be due to an
207 increase in the ThrbCRM1 RPC state, but it could also represent an increase
208 in their daughter cell production (cones, HCs, or RGCs) that could be missed
209 by the specific reporters used (Schick et al., 2019). We first examined Otx2
210 and Visinin expression to confirm the reporter-observed effects, as these

211 endogenous markers are expressed in both photoreceptors and restricted
212 RPCs (Buenaventura et al., 2018; Emerson et al., 2013). In retinas with
213 introduction of the CAG::MAML-DN construct, there was a significant increase
214 of electroporated Visinin and Otx2-labeled cells, consistent with the reporter
215 results (Fig. 3A, B). Olig2 expression, which is expected to be expressed in
216 ThrbCRM1-labeled RPCs and not cones or HCs, was significantly increased,
217 which suggests that the ThrbCRM1 reporter-positive population observed at
218 this 2 day timepoint represents the restricted RPC state (Fig. 3A and 3C)
219 (Emerson et al., 2013; Ghinia Tegla et al.; Hafler et al., 2012). In agreement
220 with this observation and the ThrbCRM2 reporter result, expression of the
221 cone gene Lhx4 was not qualitatively changed (Fig. S3B) (Buenaventura et
222 al., 2019). In contrast, the representation of the H1 HC population (marked by
223 Lim1 and AP2α; Fischer et al., 2007), normally generated by ThrbCRM1
224 restricted RPCs, is decreased in response to CAG::MAML-DN (Figure 3B). No
225 significant changes in the H2-4 HC/RGC marker Isl1 or the Brn3 family of
226 RGC markers were observed (Fig. S4) (Fischer et al., 2007; Liu et al., 2000).
227 Taken together, these data suggest that the primary effect of Notch inhibition
228 at this timepoint is to increase the formation of the restricted RPCs that
229 generate cones and HCs.
230 To further validate that these MAML-DN effects were related to Notch
231 signaling, we used flow cytometry to assess the effects of dominant-negative
232 forms of Rbpj on these same DNA reporters and cell markers. Similar effects
233 were observed upon introduction of both Rbpj-EnR and R218H constructs
234 which support the conclusion that they are a result of reduced Notch signaling
235 (Fig. S5). However, it was observed that the reduction of HCs in response to
236 the Rbpj-EnR constructs was more severe than with MAML-DN, which is
237 consistent with the Notch-independent role for Rbpj to function in a complex
238 with Ptf1a, a known regulator of HC genesis (Beres et al., 2006; Hori et al.,
239 2008; Lelièvre et al., 2011).
240

241 **Notch inhibition does not affect the number of cones produced from**
242 **restricted RPCs**

243 To test whether MAML-DN also induces a shift from HCs to cones within
244 ThrbCRM1 reporter-positive RPCs, we replaced the ubiquitous CAG promoter
245 upstream of MAML-DN with the ThrbCRM1 specific enhancer, so that MAML-
246 DN would only be expressed in ThrbCRM1-active restricted RPCs. In contrast
247 to CAG::MAML-DN, introduction of this ThrbCRM1::MAML-DN into E5 retinas
248 did not alter the number of ThrbCRM1::GFP labeled RPCs. This suggests that
249 the ectopic ThrbCRM1 cells observed with the CAG promoter are not due to
250 induction of increased proliferation within the ThrbCRM1 population. Instead,
251 this supports a role for Notch in the multipotent RPC population, in which the
252 ThrbCRM1 element is not active (Fig. 4A).

253 To genetically maintain labeling in post-mitotic daughter cells, we used a
254 lineage tracing strategy to identify the retinal cells that have a ThrbCRM1
255 history (Fig. 4B) which were previously shown to be predominantly cones and
256 H1 HCs (Schick et al., 2019). A driver plasmid was used in which the PhiC31
257 recombinase is transcriptionally regulated by the cis-regulatory element
258 ThrbCRM1. In the responder plasmid, there is a STOP codon between a
259 broadly active CAG promoter and GFP, which is flanked by two recombinase
260 target sites. Excision of the STOP sequence upon ThrbCRM1-driven
261 expression of PhiC31 recombinase, will lead to GFP expression in cells with a
262 history of ThrbCRM1 activity (Schick et al., 2019).

263 Confocal analysis of retinas electroporated with the lineage tracing
264 plasmids did not show any noticeable changes in the distribution of the
265 electroporated cells or the amount of Visinin (Fig. 4C). Flow cytometry was
266 used to quantify the percentage of cones and HCs within the GFP-labeled
267 retinal cells after two days culture. Intriguingly, the number of cone
268 photoreceptors did not change, as assessed by the expression of Visinin and
269 Otx2, while the percentage of Lim1 and AP2α-labeled HCs was reduced (Fig.
270 4D and Fig. S6A). A small percentage of Isl1-labeled HCs and Brn3-labeled

271 RGCs are formed from ThrbCRM1 restricted RPCs (Schick et al., 2019), and
272 no significant changes in the populations were detected through cell counting
273 in response to introduction of the ThrbCRM1::MAML-DN (Fig. S6B). Thus, the
274 observed reduction in HCs did not correspond to increased formation of cone
275 photoreceptors or Isl1-labeled HCs and RGCs in the daughter cell population
276 of ThrbCRM1 restricted RPCs. These unidentified cells may be other cell
277 types that cannot be identified by the cell markers used.
278

279 **Effects of MAML-DN on retinal cell proliferation and multipotency**

280 Previous analysis of mouse Notch1 conditional knockout retinas identified
281 a reduction in BrdU-positive cells, which suggested that loss of Notch
282 signaling promoted premature cell cycle exit and down-regulation of cell
283 proliferation (Jadhav et al., 2006b; Yaron et al., 2006). However, the
284 difference in the percentages of BrdU-positive cells in wild-type and Notch1
285 CKO mutant is relatively small and the reason for this effect is not known. To
286 further investigate the role of Notch in retinal cell proliferation, we co-
287 electroporated CAG::MAML-DN and CAG::TdT into E5 chick retinas and after
288 two days culture pulsed with EdU for 1 hour to label proliferating cells. We first
289 quantified the percentage of EdU/CAG::TdT double-positive cells in all the
290 electroporated cells using flow cytometry. Intriguingly, the population of
291 proliferating cells does not significantly change compared to the control (Fig.
292 5A). Introduction of the Rbpj dominant-negative construct resulted in similar
293 effects on electroporated EdU-positive cells (Fig. S7).

294 These data suggest that Notch signaling does not directly control cell
295 proliferation in retina. Although inhibition of Notch does not drastically alter the
296 overall number of RPCs within this timeframe, the experiments described
297 above suggest that it results in a shift from multipotent RPCs (decreased
298 VSX2ECR4-positive cells) to restricted RPCs (ThrbCRM1-positive cells) with
299 a significant increase in the number of ThrbCRM1/VSX2ECR4 double
300 reporter-positive cells (Fig. 2B). To confirm that these reporter-positive

301 populations are indeed proliferating, we co-electroporated ThrbCRM1 and
302 VSX2ECR4 reporters and pulsed with EdU just prior to harvest to label RPCs.
303 Flow cytometry was used to quantify the EdU/ThrbCRM1 and
304 EdU/VSX2ECR4 double-positive cells in the electroporated population. We
305 also measured the percentage of EdU/ThrbCRM1/VSX2ECR4 triple-positive
306 cells versus the combination of EdU/ThrbCRM1 and EdU/VSX2ECR4 double-
307 positive cells. There was a significant up-regulation of ThrbCRM1+/EdU+ cells
308 as well as ThrbCRM1+/VSX2ECR4+/EdU+ cells that indicated a transition
309 from VSX2ECR4-active RPCs to ThrbCRM1-active RPCs within the EdU+
310 population (Fig. 5B and 5C). In addition, immunostaining with the multipotent
311 RPC marker VSX2 showed a down-regulation of VSX2+/EdU+ cells and an
312 up-regulation of ThrbCRM1+/EdU+ cells, validating a shift between VSX2+
313 RPCs and ThrbCRM1-active RPCs (Fig. 5D).
314 To further determine if the induced ThrbCRM1 RPCs were derived from
315 multipotent RPCs, we used the VSX2ECR4 element that is active in this
316 population to drive expression of PhiC31 recombinase and conduct lineage
317 tracing of this population. The number of VSX2ECR4/ThrbCRM1 double
318 reporter-positive cells increased 5-fold in response to CAG::MAML-DN (Fig.
319 5E). This increase was consistent with the majority of new ThrbCRM1
320 reporter-positive cells being derived from multipotent RPCs, which suggests
321 that Notch inhibition specifically affects the transition from the multipotent to
322 restricted RPC state.
323
324 **Temporal parameters of the transition from multipotent RPCs to**
325 **restricted RPCs**
326 We were interested in determining the timeframe with which multipotent
327 RPCs transition to restricted RPCs. To test if the changes in multipotent RPC
328 numbers could be detected during their first cell cycle after electroporation, we
329 electroporated E5 chick retinas with VSX2ECR4::GFP, ThrbCRM1::TdT, the
330 co-electroporation reporter CAG::iRFP, and either CAG::MAML-DN or control

conditions. Retinas were harvested at 8 hours after electroporation, which is a time before multipotent RPCs would be expected to complete one cell cycle. There were no significant differences in the number of VSX2ECR4-marked multipotent RPCs or ThrbCRM1-marked restricted RPCs (Fig. 6A). In addition, the VSX2ECR4/ThrbCRM1 double reporter-positive cells were present in a very low level as observed in wild type in both MAML-DN and Rbpj-EnR mutants (Fig. 6B and Fig. S7). After 20 hours culture, the ThrbCRM1-active population started to increase slightly but not nearly as much as observed after two days (Fig. 6C). However, the transition from multipotent RPCs to restricted RPCs showed a small but significant up-regulation, as the VSX2ECR4/ThrbCRM1 double reporter-positive cells increased (Fig. 6C). Examination of Otx2 and VSX2 endogenous markers revealed a more robust response, with a decreased VSX2-positive population and an increased Otx2-positive one after 20 hours culture (Fig. 6D). Taken together, these data suggest that the RPC transition induced by Notch inhibition did not occur at 8 hours post-electroporation, but could be detected after 20 hours, and increased further at 2 days post-electroporation. This suggests that multipotent RPCs do not immediately transition to a restricted RPC state, but do so after a delay that could be accounted for by a required progression through a single, or multiple rounds, of cell division.

Increased cone genesis in response to Notch inhibition is delayed relative to restricted RPC formation

While multiple experiments support the conclusion that Notch inhibition leads to the formation of an increased restricted RPC population, we did not detect any increased cone genesis within a 2 day post-electroporation window (Fig. 2B and Fig. S3). To investigate the possibility that there is a delay in cone genesis that will occur from the induced cone/HC RPCs, we used a lineage tracing strategy to follow the fates of multipotent RPCs and assessed the cone fate within this population. Chick retinas were electroporated with a

361 VSX2ECR4::PhiC31 lineage tracing plasmid, a GFP lineage tracing reporter,
362 a ThrbCRM2::TdTomato reporter, and CAG::iRFP to mark all electroporated
363 cells (Fig. 7A). Retinal samples were harvested after two to five days culture.
364 The total number of ThrbCRM2 reporter-positive cones did not change at 2 or
365 3 days post-electroporation, however, the number of ThrbCRM2 reporter-
366 positive cells within the VSX2ECR4 lineage-traced population showed a
367 significant increase at 3 days, in line with the hypothesis that the effects of
368 Notch inhibition originate from multipotent RPCs (Fig. 7B). Both the overall
369 ThrbCRM2 population and the population specifically lineage-traced from
370 multipotent RPCs showed a very significant enrichment at 4 and 5 days after
371 electroporation (Fig. 7C), which correlated in a delayed manner with the
372 changes of ThrbCRM1 restricted RPCs from 1 to 2 days (Fig. 6C and Fig.
373 2B). This supports our hypothesis that increased cone genesis has a delay of
374 2 days relative to the up-regulated ThrbCRM1 RPCs formed in response to
375 Notch inhibition and that this increased cone cell number is ultimately caused
376 by effects that originate in multipotent RPCs.
377
378 **Discussion**
379 While critical gene regulators of retinal cell type formation have been
380 identified in the last decades, the relationships of these factors within gene
381 regulatory networks and the cellular events in which they function are much
382 less clear. One of the primary reasons for this is that, unlike other
383 developmental systems, strict lineages of cell types originating from
384 multipotent RPCs have not been identified, leading to some hypotheses that
385 this system is driven primarily by stochastic choices (Gomes et al., 2011; He
386 et al., 2012). However, identification of restricted RPC states with limited cell
387 fate potential suggests that there are at least some deterministic processes
388 involved and these are additional, discrete cellular steps in the formation of
389 specific cell types during which genes could act. Here we attempted to
390 integrate the well-documented role for the Notch pathway in the repression of

391 cone photoreceptor formation and promotion of RPC proliferation, within a
392 framework for retinal development that includes restricted RPCs.
393 We initially hypothesized that, similar to other systems, the effect of
394 Notch inhibition on cone photoreceptors would be mediated through sister cell
395 fate decisions. This would be consistent with the fact that there is a restricted
396 RPC type that primarily forms cones and HCs and that several reports that
397 examined the Notch1 mouse mutant identified an increase in cones and one
398 also reported a decrease in HCs. However, though we also detected reduced
399 HCs when we interfered with Notch signaling, we did not detect a concomitant
400 increase in photoreceptors within the ThrbCRM1 restricted RPC daughter cell
401 population. This suggests that sister cell fate choice is not the primary site of
402 functional Notch signaling during cone photoreceptor formation. The most
403 prominent and consistent effects of Notch signaling we observed were on the
404 formation of the ThrbCRM1-active restricted RPC population and a
405 concomitant depletion of the multipotent RPC population, which suggests that
406 the primary role for Notch signaling in cone formation is at the step of
407 restricted RPC derivation from multipotent RPCs. Our interpretation of these
408 results is consistent with another recent developmental study that undertook a
409 comprehensive transcriptome analysis of embryonic mouse retinas under
410 conditions of Notch inhibition (Kaufman et al., 2019). Here, it was reported
411 that the earliest effects of Notch inhibition through DAPT treatment include the
412 loss of multipotent RPC gene expression (observed as well by earlier studies
413 of Notch1 and Rbpj), but also the early increase of genes that have identified
414 primary correlations with restricted RPCs and with reduced to no expression
415 in postmitotic cones (Jadhav et al., 2006b; Riesenberg et al., 2009; Yaron et
416 al., 2006). These gene expression changes include Olig2 (Hafler et al., 2012),
417 Onecut1 (Emerson et al., 2013), and Otx2 (Emerson et al., 2013), all of which
418 have been previously shown to be expressed in restricted RPCs that give rise
419 to cones. Additional upregulated genes such as Dll4 (Rocha et al., 2009), and
420 Atoh7 (Buenaventura et al., 2018), are expressed in cycling cells and are

421 enriched in ThrbCRM1 cells as assessed by bulk RNA-Seq. All of these
422 genes displayed a temporal dynamic consistent with increased production of
423 restricted RPCs in this mouse model. In addition, several studies (Kaufman et
424 al., 2019; Nelson et al., 2007) have identified an upregulation of several
425 members of the bHLH family (NeuroD1, Ngn2, etc) which recent single cell
426 analysis has associated with neurogenic RPCs and not multipotent RPCs (Lu
427 et al., 2020).

428 A role for Notch signaling in maintaining a self-renewing multipotent
429 RPC population is also consistent with its observed effects on proliferation.
430 Many studies (Jadhav et al., 2006b; Kaufman et al., 2019; Yaron et al., 2006)
431 have identified a decrease in cycling cells when Notch signaling is inhibited.
432 We did not detect a significant decrease within two days of electroporation,
433 but consistent with other analysis at early time points in the mouse, there was
434 only a partial loss of cycling cells. Given the identified shift from multipotent to
435 restricted RPCs identified here, we would predict that the majority of the
436 remaining cycling cells in mouse Notch loss-of-function paradigms represent
437 restricted RPCs and that the loss of multipotent RPCs is actually much larger
438 than was previously assumed to be the case, as the existence of different
439 RPC populations was not known at the time of those studies. The effects of
440 Notch inhibition described here on RPC dynamics is also consistent with
441 those observed during vertebrate forebrain development, where Notch
442 inhibition leads to loss of apical progenitors and formation of intermediate
443 progenitors, preceding the appearance of postmitotic neurons (Yoon et al.,
444 2008).

445 The evidence presented in the current study, and interpreted from
446 previous ones, suggests a primary role in Notch signaling during cone
447 formation in mediation of the transition from multipotent to restricted RPC, but
448 there are critical questions that remain to be addressed. One question is how
449 cell division patterns of multipotent RPCs change with inhibition of Notch
450 signaling? Instead of a multipotent RPC dividing asymmetrically to form

451 another multipotent RPC and a ThrbCRM1 RPC, does Notch inhibition cause
452 symmetrical divisions to form two ThrbCRM1 RPCs? A recent study in the
453 zebrafish retina showed that pharmacological inhibition of Notch signaling led
454 RPCs to transition from an asymmetric mode of division to a symmetric one in
455 which two neurogenic RPCs were produced (Nerli et al., 2020). Our current
456 findings align well with those of this study, with active Notch signaling
457 functioning specifically to maintain multipotent RPCs and inhibit neurogenic
458 (what we refer to as restricted) RPC states. Previous studies have also
459 suggested that there may exist an additional RPC state located between
460 multipotent RPCs and ThrbCRM1 RPCs (Schick et al., 2019; Suzuki et al.,
461 2013). This RPC divides to form an RGC and a ThrbCRM1-like RPC on
462 division. The formation of these cells could be the first change elicited by
463 Notch inhibition which would suggest that RGCs should also increase and
464 may correspond to the Ath5+ RPCs followed in Nerli et al., 2020. We do
465 observe a number of cells in the RGC layer, however, we have not detected
466 an increase in RGCs using early RGC markers such as Islet1 and Brn3. It is
467 possible that the continued inhibition of the Notch signaling pathway in these
468 cells interferes with their differentiation. This study focused on the formation of
469 cone photoreceptors, but it will be interesting to determine if Notch functions
470 at other temporal points in retinogenesis to control the formation of other
471 restricted RPC types. Lastly, it will be informative to determine the direct
472 functional targets of Notch signaling that drive RPC transitions. Identification
473 of these pathways will have implications for our understanding of visual
474 system evolution and for the development of strategies to control the
475 proliferation dynamics and cell fate choices of stem cells for therapeutic uses.
476

477 **Methods**

478 **Animals**

479 All experimental procedures involving animals were carried out in consultation
480 with the City College of New York, CUNY Institutional Animal Care protocols.

481 Fertilized chick eggs were acquired from Charles River, stored in a 16 °C
482 room for less than 10 days and incubated in a 38 °C humidified incubator for 5
483 days. All experiments that used animals were not sex-biased.
484
485 **DNA Plasmids**
486 The Hes5::GFP reporter was provided by Dominique Henrique and described
487 in (Vilas-Boas et al., 2011). CAG::Nucβgal was obtained from the Cepko lab
488 (Cepko Lab, Harvard Medical School). Previously reported plasmids include
489 CAG::TdT (Schick et al., 2019), OC1ECR22::GFP (Patoori et al., 2020; Schick
490 et al., 2020), VSX2ECR4::GFP and CAG::iRFP (Buenaventura et al., 2018),
491 ThrbCRM1::GFP and ThrbCRM2::GFP (Emerson et al., 2013),
492 ThrbCRM1::PhiC31 and CaNa::GFP (Schick et al., 2019) and
493 CAG::AU1Gapdh (Emerson and Cepko, 2011). pCAG is vector with a CAG
494 promoter with no protein coding region downstream. To make the
495 CAG::MAML-DN plasmid (Addgene plasmid # 160923, this study), an N-
496 terminal MAML coding fragment (Weng et al., 2003) was amplified from
497 chicken cDNA and fused with a mouse Gapdh coding sequence through
498 overlap extension PCR. The PCR product was purified and digested with Age
499 Ⅰ/Nhe Ⅰ before ligation into an Age Ⅰ/Nhe Ⅰ digested CAG::AU1Gapdh
500 vector. ThrbCRM1::MAML-DN was made by replacing the CAG promoter with
501 the ThrbCRM1 element. The CAG::Rbpj-EnR (Addgene plasmid # 160924,
502 this study) and CAG::EnR-Rbpj (Addgene plasmid # 160925, this study) were
503 made by fusing mouse Rbpj (GenBank ID BC051387.1 obtained from
504 Transomic Technologies) with an engrailed repressor domain (Vickers and
505 Sharrocks, 2002) and amplification through overlap extension PCR. The
506 amplicon was digested by EcoR Ⅰ and ligated into an EcoR Ⅰ digested CAG
507 vector. The R218H mutation was introduced into a mouse CAG::Rbpj plasmid
508 through overlap extension PCR. All the plasmids described above were
509 validated by restriction digest and Sanger sequencing.
510

511 **Electroporation and Culture**

512 To deliver plasmid DNA into dissected retinas, *ex vivo* experiments were
513 carried out as described in (Emerson and Cepko, 2011) using a Nepagene
514 NEPA21 Type II Super Electroporator. DNA mixes for *ex vivo* electroporation
515 were made in 1X PBS with a final concentration of 0.1 µg/µl for the co-
516 electroporation control plasmids with CAG promoters and 0.16 µg/µl for
517 reporter and dominant-negative plasmids. Retinas were dissected at E5 and
518 cultured between 8 hours and 5 days after electroporation. In all experiments,
519 "control" refers to samples in which the same concentration of pCAG plasmid
520 was substituted for the experimental plasmid in the electroporation.

521

522 **Immunohistochemistry**

523 After harvest, retinas were fixed in 4% paraformaldehyde for 30 minutes,
524 washed 3 times in 1XPBS, and sunk in 30% sucrose/0.5XPBS overnight.
525 Retinas were frozen in OCT (Sakura Tissue-Tek, 4583). 20 µm vertical
526 sections were acquired using a Leica Cryostat and collected on 5-7 slides
527 (FisherBrand, 12-550-15).
528 Sections were blocked in 5% serum (Jackson ImmunoResearch, Donkey -
529 017-000121, Goat - 005-000-121) in 1XPBT (0.01% Tween-20 in 1XPBS) for
530 1 hour at room temperature and incubated in primary antibody at 4℃
531 overnight. The primary antibodies used were: chicken anti-GFP (ab13970,
532 Abcam, 1:2000), rabbit anti-GFP (A-6455, Invitrogen, 1:1000), chicken anti-β-
533 galactosidase (ab9361, Abcam, 1:1000), mouse IgG1 anti-β-galactosidase
534 (40-1a-s, DSHB 1:20), rabbit anti-RFP (600-401-379, Rockland, 1:250),
535 mouse IgG1 anti-Visinin (7G4-s, DSHB, 1: 500), mouse IgG1 anti-Lim1 (4F2-
536 c, DSHB, 1:30), mouse anti-AP2α (3B5, DSHB, 1:200), mouse IgG1 anti-
537 Islet1 (39.3F7, DSHB, 1:50), mouse IgG1 anti-Brn3a (MAB1585, EMD
538 Millipore, 1:800), mouse anti-Pan Brn3 (Sc-390781, Santa Cruz, 1:100),
539 sheep anti-Vsx2 (x1180p, Ex Alpha, 1:200), goat anti-Otx2 (AF1979, R&D,
540 1:500), rabbit anti-Otx2 (AB21990, Abcam, 1:500) and rabbit anti-Olig2

541 (4B9610-AF488, Millipore, 1:500). Sections were washed 3 times with 1XPBT,
542 blocked at room temperature for 30 min and incubated in secondary antibody
543 at 4℃ overnight. The secondary antibodies used were from Jackson
544 Immunoresearch and appropriate for multiple labeling. Alexa 488- and 647-
545 conjugated secondary antibodies (resuspended in 50% glycerol) were used at
546 1:400 and cy3-conjugated antibodies were used at 1:250 as described
547 (Schick et al., 2019). 4'6-diamidino-2-phenylindole (DAPI) was added at 1
548 µg/ml after 3X wash with 1XPBT. Sections were mounted using Fluoromount-
549 G (Southern Biotech, 0100-01) and 34x60 mm coverslips (VWR, 48393-106).
550

551 **EdU Labeling**

552 Before fixation, retinas were incubated at 37℃ for 1 hour with 50 µM EdU in
553 culture media and harvested as described above. Sections were
554 permeabilized for 15 minutes in 0.1% Triton in 1X PBS before incubating with
555 the EdU Reaction Cocktail for 30 minutes in the dark. Sections were washed
556 3 times with 1X PBT before blocking and antibody staining. EdU was detected
557 using a Click-iT EdU Alexa Fluor 647 imaging kit (Invitrogen, C10340).
558

559 **Confocal Microscopy and Cell Counting**

560 Confocal images were acquired using a Zeiss LSM710 inverted confocal
561 microscope with an EC Plan-Neofluar 40x/1.30 Oil DIC M27 immersion
562 objective, 488nm laser, 561 nm laser, 633 nm laser, 405 nm laser, and ZEN
563 Black 2015 21 SP2 software resolution of 1024 x 1024, acquisition speed of 6.
564 Fiji (Schindelin et al., 2012) was used to analyze images and convert into
565 picture format. Cell counting was performed using the Cell Counter plugin-in
566 for ImageJ developed by Kurt De Vos. Cell counts used at least 3 retinas for
567 each condition, 3 sections per retina. Figures were assembled using Affinity
568 Designer vector editor (Serif [Europe] Ltd). Brightness and contrast were
569 adjusted uniformly in all the figures. All retinal sections are oriented with the
570 developing photoreceptor side at the top of the image. All images are

presented as maximum projections, with the exception of Olig2-related images in Figure 3A, which are single z-planes.

Retina Dissociation and Flow Cytometry

After ex vivo culture, the remaining retinal pigment epithelium (RPE) and condensed vitreal materials were removed in HBSS (GIBCO, 14170112) and dissociated following a papain-based (Worthington, L5003126) protocol (Jean-Charles et al., 2018). Dissociated retinal cells were fixed using 4% paraformaldehyde for 15 minutes and washed 3 times in 1X PBS. Samples for quantification were filtered into 4ml tubes (BD Falcon, 352054) through 40um cell strainers (Biologix, 15-1040). Dissociated cells were analyzed with a BD LSR II flow cytometer using the 488nm, 561nm, and 633nm lasers. All flow cytometry data was analyzed using FlowJo Version 10.4.2.

Statistical Analysis

Graphs and statistical tests were conducted using Microsoft Office Excel and GraphPad Prism 8. The error bars represent S.E.M. ANOVA with a post hoc Dunn test was used in Fig. 4A and Fig. S2B. Mann-Whitney test was used in Fig. 4D, Fig. 5B, Fig 6B, Fig. S4B and Fig. S7B. A two-tailed student's t-test was used for all other statistical tests. All the tests were performed with independent samples after the Shapiro-Wilk normality test using GraphPad Prism8, and the results were significant as noted. Quantifications for flow cytometry were based on 4 biological replicates per condition and at least 2 technical replicates. Quantifications for cell counting were based on 3 biological replicates per condition with 3 sections per retina.

Acknowledgements

Funding for this project was provided by NSF CAREER 1453044 (to M.E.) and supported by NIMHD 3G12MD007603-30S2 (to CCNY). Jeffrey Walker and Jorge Morales provided technical support with flow cytometry and

confocal microcopy experiments. We thank Diego Buenaventura for providing the VSX2ECR4::PhiC31 plasmid and for guidance with flow cytometry analysis. We thank Miruna Ghinia-Tegla for advice on cell counting and Estie Schick for comments on the manuscript. Shirley Chan, Denice Moran and Boguslava Dimitrova provided technical assistance. We thank all the members of the Emerson lab for support throughout the project.

Author Contributions

XC and ME designed the experiments and analyzed the data. XC and ME conducted the experiments. XC and ME wrote the manuscript.

Competing Interests

The author(s) declare no competing interests.

616 ## References

617 Artavanis-Tsakonas, S., Delidakis, C., and Fehon, R.G. (1991). The Notch locus and the cell biology
618 of neuroblast segregation. Annu. Rev. Cell Biol. *7*, 427–452.

619 Beres, T.M., Masui, T., Swift, G.H., Shi, L., Henke, R.M., and MacDonald, R.J. (2006). PTF1 is an
620 organ-specific and Notch-independent basic helix-loop-helix complex containing the mammalian
621 Suppressor of Hairless (RBP-J) or its paralogue, RBP-L. Mol. Cell. Biol. *26*, 117–130.

622 Bray, S. (1998). Notch signalling in Drosophila: three ways to use a pathway. Semin. Cell Dev. Biol.
623 *9*, 591–597.

624 Bray, S.J. (2006). Notch signalling: a simple pathway becomes complex. Nat. Rev. Mol. Cell Biol. *7*,
625 678–689.

626 Buenaventura, D.F., Ghinia-Tegla, M.G., and Emerson, M.M. (2018). Fate-restricted retinal
627 progenitor cells adopt a molecular profile and spatial position distinct from multipotent progenitor
628 cells. Dev. Biol. *443*, 35–49.

629 Buenaventura, D.F., Corseri, A., and Emerson, M.M. (2019). Identification of Genes With Enriched
630 Expression in Early Developing Mouse Cone Photoreceptors. Invest. Ophthalmol. Vis. Sci. *60*, 2787–
631 2799.

632 Cepko, C. (2014). Intrinsically different retinal progenitor cells produce specific types of progeny.
633 Nat. Rev. Neurosci. *15*, 615–627.

634 Chung, C.N., Hamaguchi, Y., Honjo, T., and Kawaichi, M. (1994). Site-directed mutagenesis study on
635 DNA binding regions of the mouse homologue of Suppressor of Hairless, RBP-J kappa. Nucleic Acids
636 Res. *22*, 2938–2944.

637 Emerson, M.M., and Cepko, C.L. (2011). Identification of a retina-specific Otx2 enhancer element
638 active in immature developing photoreceptors. Dev. Biol. *360*, 241–255.

639 Emerson, M.M., Surzenko, N., Goetz, J.J., Trimarchi, J., and Cepko, C.L. (2013). Otx2 and Onecut1
640 promote the fates of cone photoreceptors and horizontal cells and repress rod photoreceptors.
641 Dev. Cell *26*, 59–72.

642 Fior, R., and Henrique, D. (2005). A novel hes5/hes6 circuitry of negative regulation controls Notch
643 activity during neurogenesis. Dev. Biol. *281*, 318–333.

644 Fischer, A.J., Stanke, J.J., Aloisio, G., Hoy, H., and Stell, W.K. (2007). Heterogeneity of horizontal cells
645 in the chicken retina. J. Comp. Neurol. *500*, 1154–1171.

646 Ghinia Tegla, M.G., Buenaventura, D.F., Kim, D.Y., Thakurdin, C., Gonzalez, K.C., and Emerson, M.M.
647 OTX2 represses sister cell fate choices in the developing retina to promote photoreceptor
648 specification. ELife *9*.

649 Gomes, F.L.A.F., Zhang, G., Carbonell, F., Correa, J.A., Harris, W.A., Simons, B.D., and Cayouette, M.

650 (2011). Reconstruction of rat retinal progenitor cell lineages in vitro reveals a surprising degree of
651 stochasticity in cell fate decisions. Dev. Camb. Engl. *138*, 227–235.

652 Hafler, B.P., Surzenko, N., Beier, K.T., Punzo, C., Trimarchi, J.M., Kong, J.H., and Cepko, C.L. (2012).
653 Transcription factor Olig2 defines subpopulations of retinal progenitor cells biased toward specific
654 cell fates. Proc. Natl. Acad. Sci. *109*, 7882–7887.

655 Hayes, S., Nelson, B.R., Buckingham, B., and Reh, T.A. (2007). Notch signaling regulates
656 regeneration in the avian retina. Dev. Biol. *312*, 300–311.

657 He, J., Zhang, G., Almeida, A.D., Cayouette, M., Simons, B.D., and Harris, W.A. (2012). How variable
658 clones build an invariant retina. Neuron *75*, 786–798.

659 Henrique, D., Hirsinger, E., Adam, J., Le Roux, I., Pourquié, O., Ish-Horowicz, D., and Lewis, J. (1997).
660 Maintenance of neuroepithelial progenitor cells by Delta-Notch signalling in the embryonic chick
661 retina. Curr. Biol. CB *7*, 661–670.

662 Hori, K., Cholewa-Waclaw, J., Nakada, Y., Glasgow, S.M., Masui, T., Henke, R.M., Wildner, H.,
663 Martarelli, B., Beres, T.M., Epstein, J.A., et al. (2008). A nonclassical bHLH Rbpj transcription factor
664 complex is required for specification of GABAergic neurons independent of Notch signaling. Genes
665 Dev. *22*, 166–178.

666 Jadhav, A.P., Cho, S.-H., and Cepko, C.L. (2006a). Notch activity permits retinal cells to progress
667 through multiple progenitor states and acquire a stem cell property. Proc. Natl. Acad. Sci. U. S. A.
668 *103*, 18998–19003.

669 Jadhav, A.P., Mason, H.A., and Cepko, C.L. (2006b). Notch 1 inhibits photoreceptor production in
670 the developing mammalian retina. Dev. Camb. Engl. *133*, 913–923.

671 Jean-Charles, N., Buenaventura, D.F., and Emerson, M.M. (2018). Identification and
672 characterization of early photoreceptor cis-regulatory elements and their relation to Onecut1.
673 Neural Develop. *13*, 26.

674 Kaufman, M.L., Park, K.U., Goodson, N.B., Chew, S., Bersie, S., Jones, K.L., Lamba, D.A., and
675 Brzezinski, J.A. (2019). Transcriptional profiling of murine retinas undergoing semi-synchronous
676 cone photoreceptor differentiation. Dev. Biol. *453*, 155–167.

677 Kopan, R., and Ilagan, M.X.G. (2009). The canonical Notch signaling pathway: unfolding the
678 activation mechanism. Cell *137*, 216–233.

679 Lelièvre, E.C., Lek, M., Boije, H., Houille-Vernes, L., Brajeul, V., Slembrouck, A., Roger, J.E., Sahel,
680 J.A., Matter, J.M., Sennlaub, F., et al. (2011). Ptf1a/Rbpj complex inhibits ganglion cell fate and
681 drives the specification of all horizontal cell subtypes in the chick retina. Dev. Biol. *358*, 296–308.

682 Liu, W., Khare, S.L., Liang, X., Peters, M.A., Liu, X., Cepko, C.L., and Xiang, M. (2000). All Brn3 genes
683 can promote retinal ganglion cell differentiation in the chick. Dev. Camb. Engl. *127*, 3237–3247.

684 Lu, Y., Shiau, F., Yi, W., Lu, S., Wu, Q., Pearson, J.D., Kallman, A., Zhong, S., Hoang, T., Zuo, Z., et al.
685 (2020). Single-Cell Analysis of Human Retina Identifies Evolutionarily Conserved and Species-
686 Specific Mechanisms Controlling Development. Dev. Cell *53*, 473-491.e9.

687 Mizeracka, K., Trimarchi, J.M., Stadler, M.B., and Cepko, C.L. (2013a). Analysis of Gene Expression
688 in Wild-Type and Notch1 Mutant Retinal Cells by Single Cell Profiling. Dev. Dyn. Off. Publ. Am. Assoc.
689 Anat. *242*.

690 Mizeracka, K., DeMaso, C.R., and Cepko, C.L. (2013b). Notch1 is required in newly postmitotic cells
691 to inhibit the rod photoreceptor fate. Dev. Camb. Engl. *140*, 3188–3197.

692 Mumm, J.S., and Kopan, R. (2000). Notch signaling: from the outside in. Dev. Biol. *228*, 151–165.

693 Nelson, B.R., Hartman, B.H., Georgi, S.A., Lan, M.S., and Reh, T.A. (2007). Transient inactivation of
694 Notch signaling synchronizes differentiation of neural progenitor cells. Dev. Biol. *304*, 479–498.

695 Nerli, E., Rocha-Martins, M., and Norden, C. (2020). Asymmetric neurogenic commitment of retinal
696 progenitors involves Notch through the endocytic pathway. ELife *9*.

697 Patoori, S., Jean-Charles, N., Gopal, A., Sulaiman, S., Gopal, S., Wang, B., Souferi, B., and Emerson,
698 M.M. (2020). Cis-regulatory analysis of Onecut1 expression in fate-restricted retinal progenitor
699 cells. Neural Develop. *15*, 5.

700 Riesenberg, A.N., Liu, Z., Kopan, R., and Brown, N.L. (2009). Rbpj cell autonomous regulation of
701 retinal ganglion cell and cone photoreceptor fates in the mouse retina. J. Neurosci. Off. J. Soc.
702 Neurosci. *29*, 12865–12877.

703 Rocha, S.F., Lopes, S.S., Gossler, A., and Henrique, D. (2009). Dll1 and Dll4 function sequentially in
704 the retina and pV2 domain of the spinal cord to regulate neurogenesis and create cell diversity.
705 Dev. Biol. *328*, 54–65.

706 Schick, E., McCaffery, S.D., Keblish, E.E., Thakurdin, C., and Emerson, M.M. (2019). Lineage tracing
707 analysis of cone photoreceptor associated cis-regulatory elements in the developing chicken retina.
708 Sci. Rep. *9*, 1–14.

709 Schick, E., Gonzalez, K.C., Dutta, P., Hossain, K., Tegla, M.G.G., and Emerson, M.M. (2020). Early cis-
710 regulatory events in the formation of retinal horizontal cells. BioRxiv 2020.12.02.409003.

711 Schindelin, J., Arganda-Carreras, I., Frise, E., Kaynig, V., Longair, M., Pietzsch, T., Preibisch, S.,
712 Rueden, C., Saalfeld, S., Schmid, B., et al. (2012). Fiji: an open-source platform for biological-image
713 analysis. Nat. Methods *9*, 676–682.

714 Shevtsova, Z., Malik, J.M.I., Michel, U., Schöll, U., Bähr, M., and Kügler, S. (2006). Evaluation of
715 epitope tags for protein detection after in vivo CNS gene transfer. Eur. J. Neurosci. *23*, 1961–1969.

716 Suzuki, S.C., Bleckert, A., Williams, P.R., Takechi, M., Kawamura, S., and Wong, R.O.L. (2013). Cone
717 photoreceptor types in zebrafish are generated by symmetric terminal divisions of dedicated

718 precursors. Proc. Natl. Acad. Sci. U. S. A. *110*, 15109–15114.

719 Tan, G.C., Mazzoni, E.O., and Wichterle, H. (2016). Iterative Role of Notch Signaling in Spinal Motor
720 Neuron Diversification. Cell Rep. *16*, 907–916.

721 Vickers, E.R., and Sharrocks, A.D. (2002). The use of inducible engrailed fusion proteins to study
722 the cellular functions of eukaryotic transcription factors. Methods San Diego Calif *26*, 270–280.

723 Vilas-Boas, F., Fior, R., Swedlow, J.R., Storey, K.G., and Henrique, D. (2011). A novel reporter of notch
724 signalling indicates regulated and random Notch activation during vertebrate neurogenesis. BMC
725 Biol. *9*, 58.

726 Weng, A.P., Nam, Y., Wolfe, M.S., Pear, W.S., Griffin, J.D., Blacklow, S.C., and Aster, J.C. (2003).
727 Growth suppression of pre-T acute lymphoblastic leukemia cells by inhibition of notch signaling.
728 Mol. Cell. Biol. *23*, 655–664.

729 Wu, L., Aster, J.C., Blacklow, S.C., Lake, R., Artavanis-Tsakonas, S., and Griffin, J.D. (2000). MAML1,
730 a human homologue of Drosophila mastermind, is a transcriptional co-activator for NOTCH
731 receptors. Nat. Genet. *26*, 484–489.

732 Yaron, O., Farhy, C., Marquardt, T., Applebury, M., and Ashery-Padan, R. (2006). Notch1 functions
733 to suppress cone-photoreceptor fate specification in the developing mouse retina. Dev. Camb. Engl.
734 *133*, 1367–1378.

735 Yoon, K.-J., Koo, B.-K., Im, S.-K., Jeong, H.-W., Ghim, J., Kwon, M., Moon, J.-S., Miyata, T., and Kong,
736 Y.-Y. (2008). Mind Bomb 1-Expressing Intermediate Progenitors Generate Notch Signaling to
737 Maintain Radial Glial Cells. Neuron *58*, 519–531.

738

739 **Figure Legends**

740 **Fig. 1.** CAG::MAML-DN inhibits the expression of the Hes5 Notch reporter
741 **A.** Schematic representation of the electroporation paradigm with plasmids
742 introduced ex vivo into E5 chick retinas, cultured for two days, dissociated into
743 single cells and analyzed by flow cytometry. A schematic of the MAML
744 dominant-negative construct is shown. **B.** Confocal images of vertically
745 sectioned E5 chick retinas co-electroporated with CAG::Nucßgal, Hes5::GFP
746 Notch reporter, and with or without CAG::MAML-DN and then cultured for two
747 days. The scale bar shown in the bottom right picture denotes 40 μm and
748 applies to all images. All images are oriented with the scleral side of the retina
749 at the top of the image. **C.** Flow cytometry dot plots of dissociated chick
750 retinal cells electroporated *ex vivo* at E5 with a co-electroporation control
751 (CAG::iRFP), Hes5::GFP, and with or without CAG::MAML-DN. The bar graph
752 on the right shows the percentage of Hes5::GFP reporter-positive cells within
753 the electroporated population. The Shapiro-Wilk normality test was used to
754 confirm the normal distribution. ** signifies $p<0.01$ with a two-tailed student's t-
755 test. Each point represents one biological replicate.

756

757 **Fig. 2.** CAG::MAML-DN induced Notch inhibition promotes ThrbCRM1
758 restricted RPC formation
759 **A.** Confocal images of vertically sectioned E5 chick retinas co-electroporated
760 with CAG::Nucßgal, either ThrbCRM1 or VSX2ECR4 GFP reporters, and with
761 or without CAG::MAML-DN and then cultured for two days. The scale bar
762 shown in the bottom right picture denotes 40 μm and applies to all images. All
763 images are oriented with the scleral side of the retina at the top of the image.
764 **B.** Flow cytometry quantification of the percentage of ThrbCRM1::TdTomato,
765 ThrbCRM2::TdTomato, VSX2ECR4::GFP and OC1ECR22::GFP reporter-
766 positive cells within the CAG::iRFP electroporated population in E5 retinas
767 cultured for two days. Green bars represent control conditions and yellow bars
768 inclusion of the CAG::MAML-DN construct. The Shapiro-Wilk normality test

769 was used to confirm the normal distribution. * signifies p<0.05, ** signifies
770 p<0.01, *** signifies p<0.001 with a two-tailed student's t-test. Each point
771 represents one biological replicate.
772
773 **Fig. 3.** Effects of CAG::MAML-DN on endogenous retinal markers
774 **A.** Confocal images of vertically sectioned E5 chick retinas co-electroporated
775 with CAG::Nucßgal, and with or without CAG::MAML-DN and then cultured for
776 two days. Sections were immunostained with Otx2 or Olig2 markers
777 (magenta), CAG::Nucßgal (yellow), and nuclei visualized with DAPI. The
778 scale bar shown in the bottom right picture denotes 40 μm and applies to all
779 images. All images are oriented with the scleral side of the retina at the top of
780 the image. **B.** Flow cytometry quantification of the percentage of Visinin,
781 Otx2, Lim1 and AP2α -positive cells within the electroporated cells.
782 Dissociated chick retinal cells electroporated *ex vivo* at E5 with the co-
783 electroporation control CAG::TdTomato, under control (green bars) or
784 CAG::MAML-DN (yellow bars) conditions. The retinas were cultured for two
785 days. The Shapiro-Wilk normality test was used to confirm the normal
786 distribution. ** signifies p<0.01, *** signifies p<0.001 with a two-tailed
787 student's t-test. Each point represents one biological replicate. **C.**
788 Quantification of the percentage of Olig2-positive cells within the
789 electroporated cell population from cell counting. Sectioned chick retinas
790 electroporated *ex vivo* at E5 with the co-electroporation control
791 CAG::Nucßgal. The retinas were cultured for two days. The Shapiro-Wilk
792 normality test was used to confirm the normal distribution. *** signifies
793 p<0.001 with a two-tailed student's t-test. Each point represents one biological
794 replicate.
795
796 **Fig. 4.** Targeted expression of MAML-DN to cone/HC restricted RPCs does
797 not alter cone formation

798 **A.** Flow cytometry quantification of the percentage of ThrbCRM1::GFP
799 reporter-positive cells within all the electroporated cells. Dissociated chick
800 retinal cells electroporated *ex vivo* at E5 with the CAG::iRFP co-
801 electroporation control, and with or without CAG::MAML-DN or
802 ThrbCRM1::MAML-DN and cultured for two days. The Shapiro-Wilk normality
803 test was used to confirm the normal distribution. ANOVA with a post hoc Dunn
804 test was used to test significance. ** signifies $p<0.01$, ns signifies $p>0.05$.
805 **B.** Schematic representation of PhiC31 recombinase-based lineage tracing
806 strategy (Schick et al., 2019). **C.** Confocal images of vertically sectioned E5
807 chick retinas co-electroporated with CAG::Nucßgal using ThrbCRM1::MAML-
808 DN lineage trace with a PhiC31 responder plasmid shown in A. The retinas
809 were cultured for two days post-electroporation. Sections were
810 immunostained with Visinin (magenta), CAG::Nucßgal (orange), and nuclei
811 visualized with DAPI. The scale bar shown in the bottom right picture denotes
812 40 µm and applies to all images. All images are oriented with the scleral side
813 of the retina at the top of the image. **D.** Flow cytometry quantification of the
814 percentage of Otx2, Lim1, AP2α, OC1ECR22 and ThrbCRM2 reporter-
815 positive cells within the ThrbCRM1 lineage traced cell population. Dissociated
816 chick retinal cells electroporated *ex vivo* at E5 with the co-electroporation
817 control CAG::TdTomato, ThrbCRM1::PhiC31 and its responder plasmid, and
818 with or without CAG::MAML-DN. The retinas were cultured for two days post-
819 electroporation. The Shapiro-Wilk normality test was used to confirm the
820 normal distribution. Mann-Whitney test was used to test significance in
821 ThrbCRM2 quantification. A two-tailed student's t-test was used to test
822 significance in the rest of the quantifications. * signifies $p<0.05$, ** signifies
823 $p<0.01$. Each point represents one biological replicate.
824
825 **Fig. 5.** CAG::MAML-DN induced Notch inhibition leads to a shift from
826 multipotent to cone/HC restricted RPCs

827 **A.** Flow cytometry quantification of the percentage of EdU-positive cells within
828 the electroporated cell population. Dissociated chick retinal cells
829 electroporated *ex vivo* at E5 with the co-electroporation control
830 CAG::TdTomato with or without CAG::MAML-DN. The retinas were cultured
831 for two days after electroporation and pulsed with EdU for 1 hour before
832 harvest. The Shapiro-Wilk normality test was used to confirm the normal
833 distribution. A two-tailed student's t-test was used to test significance. **B.**
834 Flow cytometry quantification of EdU+ cells positive for VSX2ECR4::GFP or
835 ThrbCRM1::TdTomato reporters. Dissociated chick retinal cells electroporated
836 *ex vivo* at E5 with VSX2ECR4::GFP and ThrbCRM1::TdTomato. The retinas
837 were cultured for two days after electroporation and pulsed with EdU for 1
838 hour before harvest. The Shapiro-Wilk normality test was used to confirm the
839 normal distribution. Mann-Whitney test was used to test significance in
840 VSX2ECR4::GFP/EdU+ quantification. A two-tailed student's t-test was used
841 to test significance in ThrbCRM1::TdTomato/EdU+ quantification. ** signifies
842 $p<0.01$. **C.** Flow cytometry quantification of ThrbCRM1::TdTomato reporter-
843 positive cells that also express VSX2ECR4::GFP reporter and EdU from
844 dissociated chick retinal cells electroporated *ex vivo* at E5 with
845 VSX2ECR4::GFP and ThrbCRM1::TdTomato. Retinas were cultured for two
846 days and pulsed with EdU for 1 hour prior to harvest. The Shapiro-Wilk
847 normality test was used to confirm the normal distribution. *** signifies
848 $p<0.001$ with a two-tailed student's t-test. **D.** Confocal images of vertically
849 sectioned E5 chick retinas co-electroporated with CAG::Nucßgal,
850 ThrbCRM1::GFP or VSX2ECR4::GFP, and with or without CAG::MAML-DN.
851 The retinas were cultured for two days after electroporation and pulsed with
852 EdU for 1 hour before harvest. The sections were immunostained with VSX2
853 maker (green), CAG::Nucßgal (orange), and nuclei visualized with DAPI. The
854 scale bar shown in the bottom right picture denotes 40 μm and applies to all
855 images. All images are oriented with the scleral side of the retina at the top of
856 the image. **E.** Flow cytometry quantification of the percentage of

857 VSX2ECR4/ThrbCRM1 double reporter-positive cells within the VSX2ECR4
858 lineage traced population. Dissociated chick retinal cells electroporated *ex*
859 *vivo* at E5 with the co-electroporation control CAG::iRFP, VSX2ECR4::PhiC31
860 and its responder plasmid, and with or without CAG::MAML-DN. The retinas
861 were cultured for two days post-electroporation. The Shapiro-Wilk normality
862 test was used to confirm the normal distribution. ** signifies p<0.01 with a two-
863 tailed student's t-test. Each point represents one biological replicate.
864
865 **Fig. 6.** The short-term effects of Notch inhibition on RPC reporters
866 **A.** Confocal images of vertically sectioned E5 chick retinas co-electroporated
867 with CAG::Nucßgal, ThrbCRM1::GFP or VSX2ECR4::GFP, and with or
868 without CAG::MAML-DN. The retinas were cultured for 8 hours post-
869 electroporation. The scale bar shown in the bottom right picture denotes 40
870 µm and applies to all images. All images are oriented with the scleral side of
871 the retina at the top of the image. **B.** Flow cytometry quantification of the
872 percentage of VSX2ECR4, ThrbCRM1 and VSX2ECR4/ThrbCRM1 reporter-
873 positive cells within all the electroporated cells. Dissociated chick retinal cells
874 electroporated *ex vivo* at E5 with the co-electroporation control CAG::iRFP
875 with or without CAG::MAML-DN. The retinas were cultured for 8 hours post-
876 electroporation. The Shapiro-Wilk normality test was used to confirm the
877 normal distribution. Mann-Whitney test was used to test significance in
878 VSX2ECR4 quantification. A two-tailed student's t-test was used to test
879 significance in ThrbCRM1 and double-positive quantifications. **C.** Flow
880 cytometry quantification of the percentage of VSX2ECR4, ThrbCRM1 and
881 VSX2ECR4/ThrbCRM1 reporter-positive cells within all the electroporated
882 cells. Dissociated chick retinal cells electroporated with CAG::iRFP *ex vivo* at
883 E5 and cultured for 20 hours. The Shapiro-Wilk normality test was used to
884 confirm the normal distribution. *** signifies p<0.001 with a two-tailed
885 student's t-test. Each point represents one biological replicate. **D.**
886 Quantification of the percentage of VSX2, Otx2 and double marker-positive

887 cells within the electroporated cell population from cell counting. Sectioned
888 chick retinas electroporated *ex vivo* at E5 with the co-electroporation control
889 CAG::Nucßgal with or without CAG::MAML-DN. The retinas were cultured for
890 20 hours and immunostained with VSX2 or Otx2 antibodies. The Shapiro-Wilk
891 normality test was used to confirm the normal distribution. * signifies $p<0.05$,
892 *** signifies $p<0.001$ with a two-tailed student's t-test. Each point represents
893 one biological replicate.
894
895 **Fig. 7.** Notch inhibition leads to a delayed increase in cones relative to
896 cone/HC RPCs
897 **A.** Schematic of experimental set-up. Retinas were electroporated with
898 VSX2ECR4::PhiC31 and CAG::stopGFP responder plasmid to label
899 multipotent RPCs (mpRPC)s and their descendents. In addition,
900 ThrbCRM2::TdT was co-electroporated to identify a subset of cones.
901 CAG::MAML-DN was included in experimental conditions and omitted in
902 control conditions. CAG::iRFP was included as a co-electroporation control
903 (not shown). Retinas were assessed 2 to 5 days later by flow cytometry to
904 measure GFP, TdT, and iRFP activity. Non-electroporated cells are shown in
905 blue, lineage-traced cells other than cones in green, non-lineage traced
906 ThrbCRM2+ cells in magenta and lineage traced ThrbCRM2+ cells in orange.
907 **B.** Flow cytometry quantification of the percentage of ThrbCRM2::TdTomato
908 reporter-positive cells within all the electroporated cells using VSX2ECR4
909 lineage trace strategy with the PhiC31 responder plasmid shown in Fig. 4B.
910 Dissociated chick retinal cells electroporated *ex vivo* at E5 with the co-
911 electroporation control CAG::iRFP, VSX2ECR4::PhiC31 and its responder
912 plasmid, ThrbCRM2::TdTomato, and with or without CAG::MAML-DN. The
913 retinas were cultured for 2 or 3 days post-electroporation. A two-tailed
914 student's t-test was used to test significance. The Shapiro-Wilk normality test
915 was used to confirm the normal distribution. * signifies $p<0.05$, ** signifies
916 $p<0.01$, *** signifies $p<0.001$ with a two-tailed student's t-test. Each point

917 represents one biological replicate. **C.** Same as A but with 4 or 5 days
918 culture.
919
920 **Fig. 8.** Model of Notch inhibition effects on cone/HC regulatory network
921 Schematic of the general relationship between multipotent RPCs (mpRPC,
922 beige), cone/HC RPCs (green), cones (blue), and HCs (purple). Grey shading
923 denotes cell-type limits of Notch inhibition. CAG::MAML-DN is broadly active
924 in all cells (denoted by grey shading) and leads to reduction in mpRPCs,
925 increase in cone/HC RPCs and cones. Bottom graphs represent relative
926 numbers of cell type populations under control and Notch inhibition conditions.
927 Dotted lines represent decreased numbers.
928
929 **Fig. S1.** CAG::MAML-DN expression and validation in retinal cells
930 **A.** Confocal images of vertically sectioned E5 chick retinas co-electroporated
931 with CAG::Nucßgal, Hes5::GFP, and with CAG::MAML-DN or empty AU1-
932 Gapdh vector and cultured for two days before AU1 immunostaining. The
933 scale bar shown in the bottom right picture denotes 40 μm and applies to all
934 images. All images are oriented with the scleral side of the retina at the top of
935 the image. **B.** Bar graphs of flow cytometry analysis of dissociated chick
936 retinal cells electroporated *ex vivo* at E5 with the CAG::iRFP co-
937 electroporation control, Hes5::GFP reporter, ThrbCRM1::TdT, and with
938 CAG::MAML-DN or empty AU1-Gapdh vector and cultured for two days. The
939 number of reporter-positive cells within the electroporated population is
940 plotted. The Shapiro-Wilk normality test was used to confirm the normal
941 distribution. *** signifies $p<0.001$ with a two-tailed student's t-test. Each point
942 represents one biological replicate.
943
944 **Fig. S2.** Rbpj-EnR and R218H have similar effects as CAG::MAML-DN on
945 Hes5 Notch reporter

946 **A.** Confocal images of vertically sectioned E5 chick retinas co-electroporated
947 with CAG::Nucßgal, Hes5::GFP Notch reporter, and with or without Rbpj-EnR
948 and cultured for two days before immunostained with Visinin. The scale bar
949 shown in the bottom right picture denotes 40 μm and applies to all images. All
950 images are oriented with the scleral side of the retina at the top of the image.
951 **B.** Flow cytometry quantification of the percentage of Hes5::GFP-positive cells
952 within all the electroporated cells. Dissociated chick retinal cells
953 electroporated *ex vivo* at E5 with the CAG::iRFP co-electroporation control,
954 Hes5::GFP, and with or without EnR-Rbpj or Rbpj-EnR and cultured for two
955 days. The Shapiro-Wilk normality test was used to confirm the normal
956 distribution. ANOVA with a post hoc Dunn test was used to test significance.
957 *** signifies $p<0.001$. Each point represents one biological replicate. **C.**
958 Same as A but with or without R218H.
959
960 **Fig. S3.** CAG::MAML-DN does not promote cone formation at two days post-
961 electroporation
962 **A.** Confocal images of vertically sectioned E5 chick retinas co-electroporated
963 with CAG::Nucßgal, ThrbCRM2::GFP or OC1ECR22::GFP, and with or
964 without CAG::MAML-DN and cultured for two days. The scale bar shown in
965 the bottom right picture denotes 40 μm and applies to all images. All images
966 are oriented with the scleral side of the retina at the top of the image. **B.**
967 Confocal images of vertically sectioned E5 chick retinas co-electroporated
968 with CAG::Nucßgal, ThrbCRM1::GFP , and with or without CAG::MAML-DN
969 and cultured for two days. LHX4 antibody was used to label cones. The scale
970 bar shown in the bottom right picture denotes 40 μm and applies to all
971 images. All images are oriented with the scleral side of the retina at the top of
972 the image.
973
974 **Fig. S4.** CAG::MAML-DN does not shift the number of H2, H3 and H4 HCs
975 and RGCs

976 **A.** Confocal images of vertically sectioned E5 chick retinas co-electroporated
977 with CAG::Nucßgal, and with or without CAG::MAML-DN and cultured for two
978 days. Sections were immunostained with Islet1 and Pan Brn3 cell specific
979 markers (magenta), CAG::Nucßgal (orange), and nuclei visualized with DAPI.
980 The scale bar in the bottom right panel denotes 40 μm and applies to all
981 images. All images are oriented with the scleral side of the retina at the top of
982 the image. **B.** Flow cytometry quantification of the percentage of Islet1,
983 Brn3a and Pan Brn3-positive cells within all electroporated cells. Dissociated
984 chick retinal cells electroporated *ex vivo* at E5 with the CAG::TdTomato co-
985 electroporation control and cultured for two days. The Shapiro-Wilk normality
986 test was used to confirm the normal distribution. A two-tailed student's t-test
987 was used to test significance in Islet1 and Brn3a quantifications. Mann-
988 Whitney test was used to test significance in Pan Brn3 quantification. Each
989 point represents one biological replicate.
990
991 **Fig. S5.** Rbpj-EnR and R218H have similar effects as CAG::MAML-DN on
992 ThrbCRM1 RPCs
993 **A.** Flow cytometry quantification of the percentage of VSX2ECR4::GFP,
994 ThrbCRM1::TdTomato, VSX2ECR4::GFP/ThrbCRM1::TdTomato double
995 reporter-positive, Visinin, ThrbCRM2::TdTomato, OC1ECR22::GFP, Lim1 and
996 AP2α -positive cells within all the electroporated cells. Dissociated chick
997 retinal cells electroporated *ex vivo* at E5 with the CAG::iRFP or
998 CAG::TdTomato co-electroporation control, and with or without Rbpj-EnR and
999 cultured for two days. The Shapiro-Wilk normality test was used to confirm the
1000 normal distribution. ** signifies $p<0.01$, *** signifies $p<0.001$ with a two-tailed
1001 student's t-test. **B.** Flow cytometry quantification of the percentage of
1002 ThrbCRM2::TdTomato, VSX2ECR4::GFP, ThrbCRM1::TdTomato,
1003 VSX2ECR4::GFP/ThrbCRM1::TdTomato double reporter-positive cells within
1004 all the electroporated cells. Dissociated chick retinal cells electroporated *ex*
1005 *vivo* at E5 with the CAG::iRFP co-electroporation control, and with or without

1006 R218H and cultured for two days. The Shapiro-Wilk normality test was used
1007 to confirm the normal distribution. ANOVA with a post hoc Dunn test was used
1008 to test significance. * signifies $p<0.05$. Each point represents one biological
1009 replicate.
1010
1011 **Fig. S6.** ThrbCRM1::MAML-DN does not have effects on H2, H3 and H4 HCs
1012 and RGCs within ThrbCRM1 lineage traced population
1013 **A.** Confocal images of vertically sectioned E5 chick retinas co-electroporated
1014 with CAG::Nucßgal, ThrbCRM1::PhiC31 and its responder plasmid, and with
1015 or without ThrbCRM1::MAML-DN. The retinas were cultured for two days
1016 post-electroporation. The sections were immunostained with Otx2, Lim1 and
1017 AP2α markers (magenta), CAG::Nucßgal (orange), and nuclei visualized
1018 with DAPI. The scale bar shown in the bottom right picture denotes 40 μm and
1019 applies to all images. All images are oriented with the scleral side of the retina
1020 at the top of the image. **B.** Quantification of the percentage of Islet1 and
1021 Brn3 marker-positive cells within the ThrbCRM1 lineage traced cell population
1022 from cell counting. Sectioned chick retinas electroporated *ex vivo* at E5 with
1023 the co-electroporation control CAG::Nucßgal, ThrbCRM1::PhiC31 and its
1024 responder plasmid, and with or without ThrbCRM1::MAML-DN. The retinas
1025 were cultured for two days after electroporation. The Shapiro-Wilk normality
1026 test was used to confirm the normal distribution. A two-tailed student's t-test
1027 was used to test significance. Each point represents one biological replicate.
1028
1029 **Fig. S7.** Rbpj-EnR induced Notch inhibition has similar effects as
1030 CAG::MAML-DN on cell proliferation
1031 **A.** Flow cytometry quantification of the percentage of EdU-positive cells within
1032 all the electroporated cells. Dissociated chick retinal cells electroporated *ex*
1033 *vivo* at E5 with the co-electroporation control CAG::TdTomato with or without
1034 Rbpj-EnR. The retinas were cultured for two days after electroporation and
1035 pulsed with EdU for 1 hour before harvest. The Shapiro-Wilk normality test

1036 was used to confirm the normal distribution. A two-tailed student's t-test was
1037 used to test significance. **B.** Flow cytometry quantification of the percentage
1038 of VSX2ECR4, ThrbCRM1 or VSX2ECR4/ThrbCRM1 reporter-positive cells
1039 within the electroporated cell population. Dissociated chick retinal cells
1040 electroporated *ex vivo* at E5 with the co-electroporation control CAG::iRFP,
1041 VSX2ECR4::GFP or ThrbCRM1::TdTomato, and with or without Rbpj-EnR.
1042 The retinas were cultured for 8 hours post-electroporation. The Shapiro-Wilk
1043 normality test was used to confirm the normal distribution. A two-tailed
1044 student's t-test was used to test significance in ThrbCRM1 quantification.
1045 Mann-Whiteney test was used to test significance in VSX2ECR4 and double
1046 reporter-positive quantifications. * signifies $p<0.05$. Each point represents one
1047 biological replicate.

Fig. 1

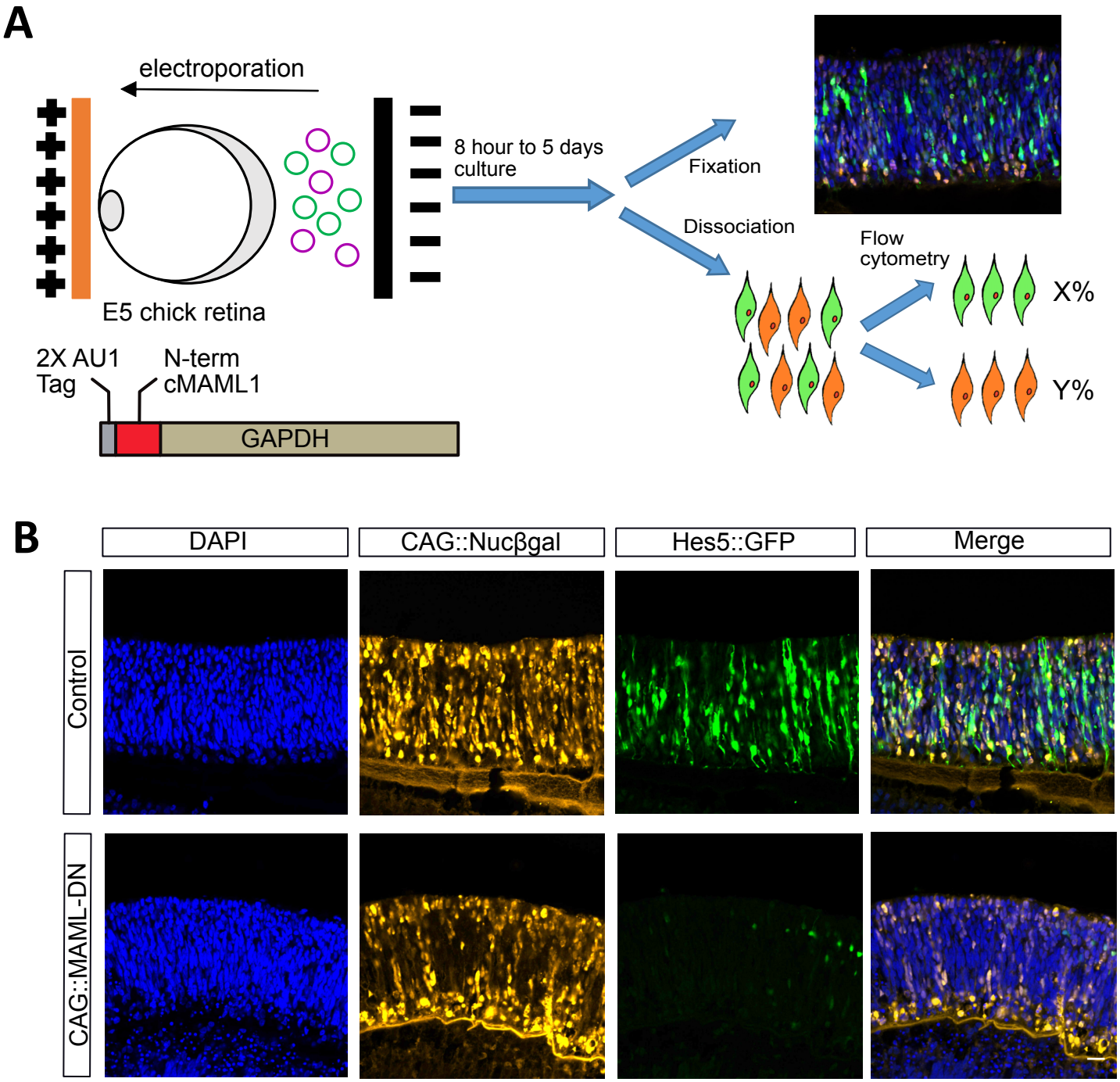
A
electroporation
E5 chick retina
8 hour to 5 days culture
Fixation
Dissociation
Flow cytometry
X%
Y%
2X AU1 Tag
N-term cMAML1
GAPDH
B
DAPI
CAG::Nucβgal
Hes5::GFP
Merge
Control
CAG::MAML-DN

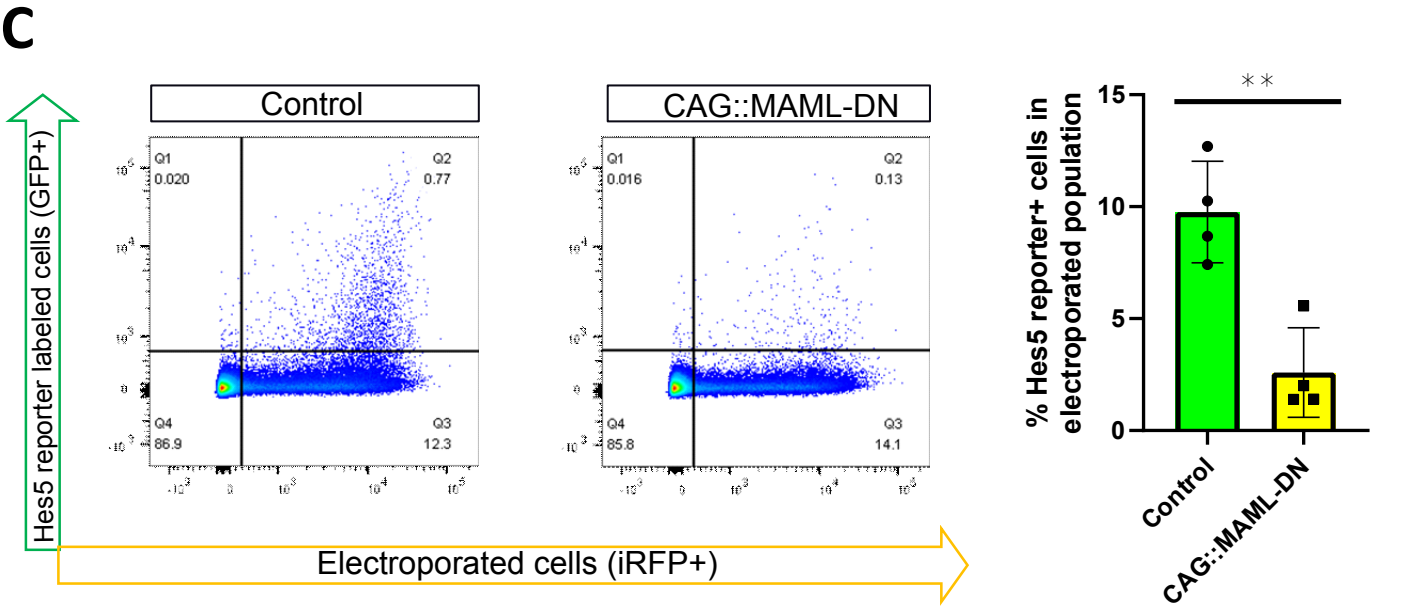
C
Control
CAG::MAML-DN
Q1 0.020
Q2 0.77
Q4 86.9
Q3 12.3
Q1 0.016
Q2 0.13
Q4 85.8
Q3 14.1
Hes5 reporter labeled cells (GFP+)
Electroporated cells (iRFP+)
% Hes5 reporter+ cells in electroporated population
15
10
5
0
**
Control
CAG::MAML-DN

Fig. 2

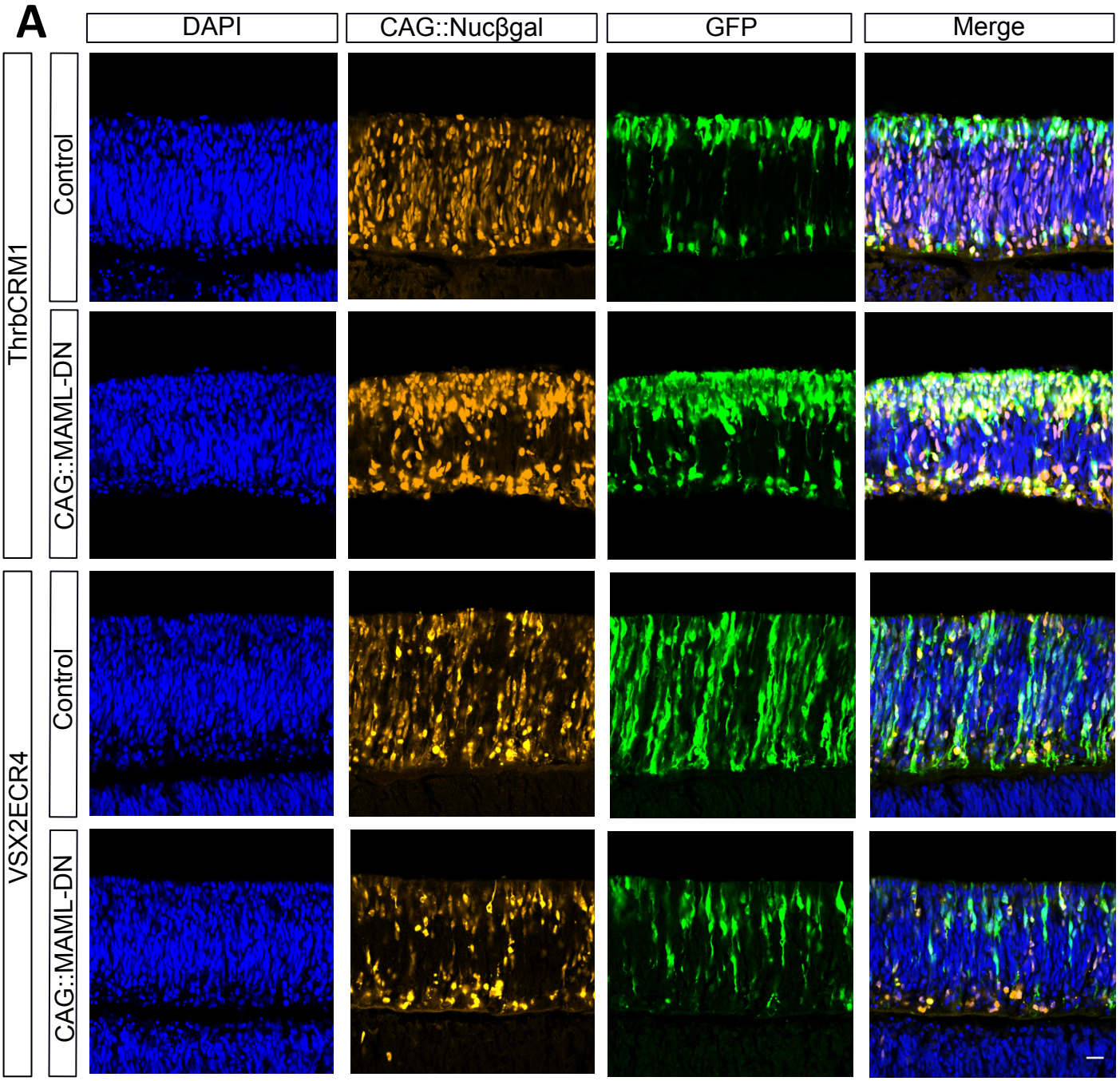
A
DAPI
CAG::Nucβgal
GFP
Merge
ThrbCRM1
Control
CAG::MAML-DN
VSX2ECR4
Control
CAG::MAML-DN

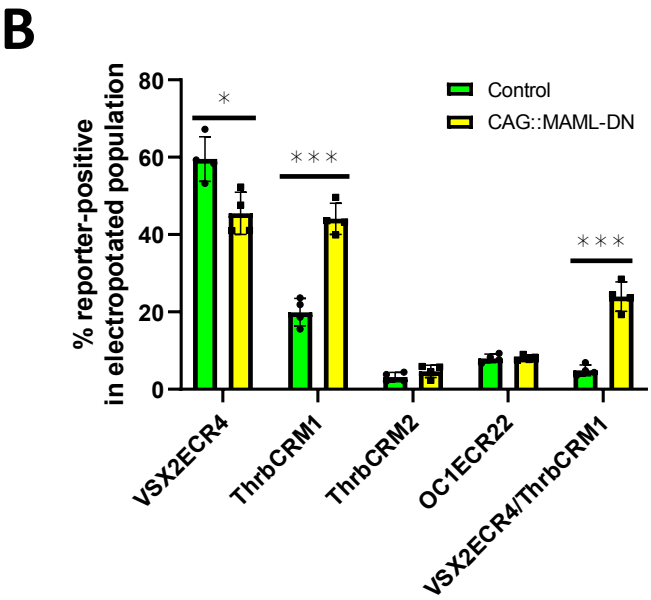
B
% reporter-positive in electropotated population
80
60
40
20
0
Control
CAG::MAML-DN
*
***
***
VSX2ECR4
ThrbCRM1
ThrbCRM2
OC1ECR22
VSX2ECR4/ThrbCRM1

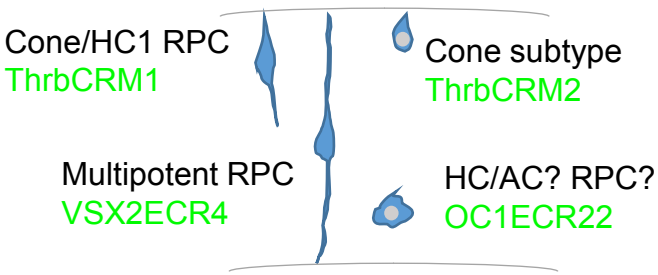
Cone/HC1 RPC
ThrbCRM1
Cone subtype
ThrbCRM2
Multipotent RPC
VSX2ECR4
HC/AC? RPC?
OC1ECR22

Fig. 3

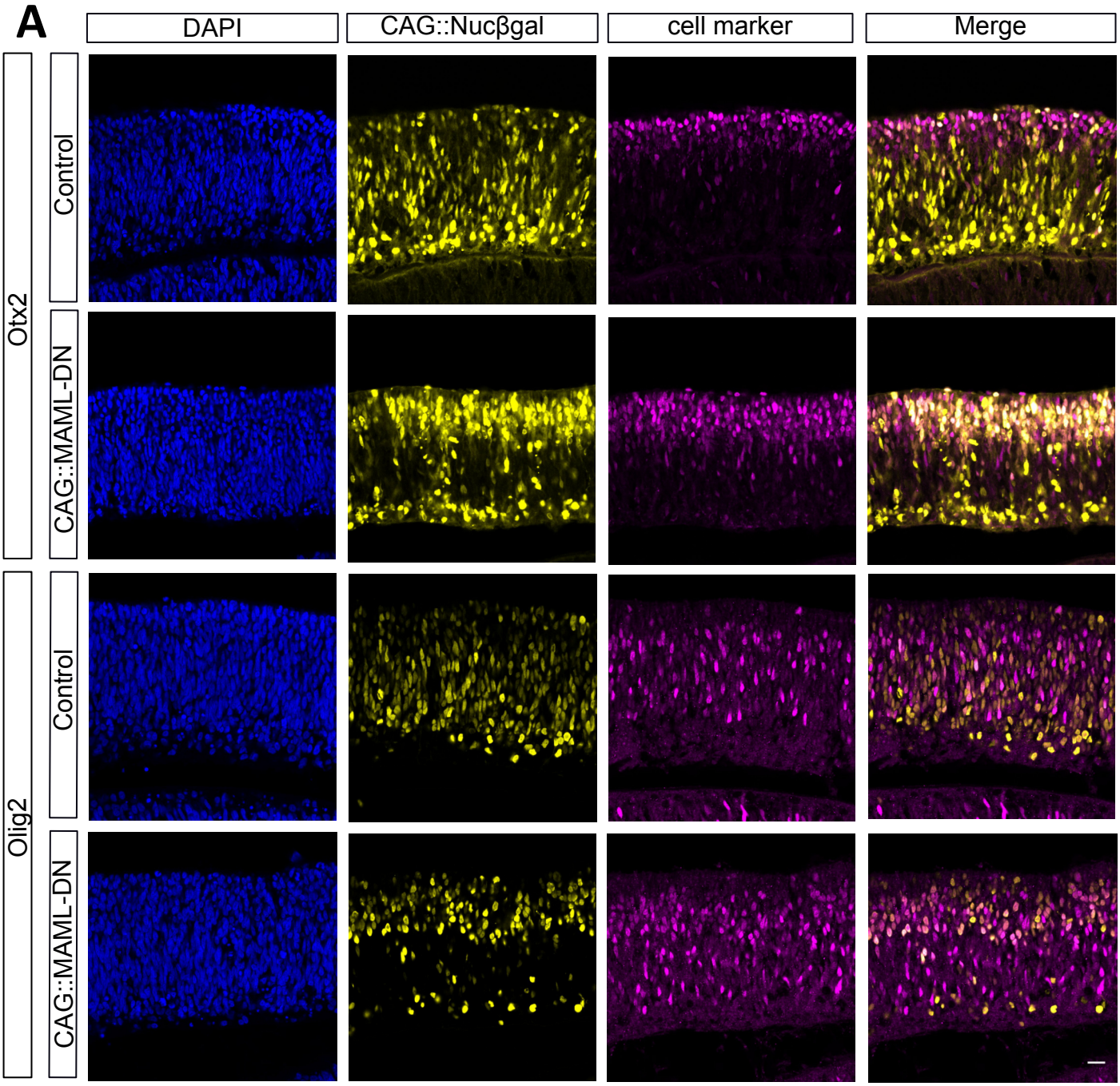
A
DAPI
CAG::Nucβgal
cell marker
Merge
Otx2
Control
CAG::MAML-DN
Olig2
Control
CAG::MAML-DN

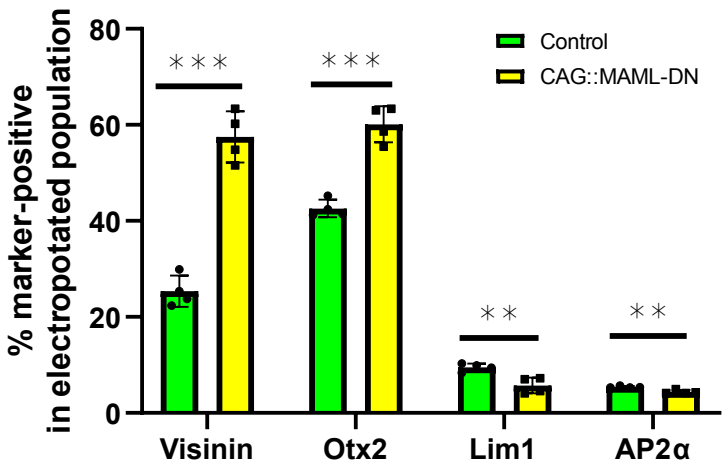
B
% marker-positive
in electropotated population
80
60
40
20
0
***
***
**
**
Control
CAG::MAML-DN
Visinin
Otx2
Lim1
AP2α

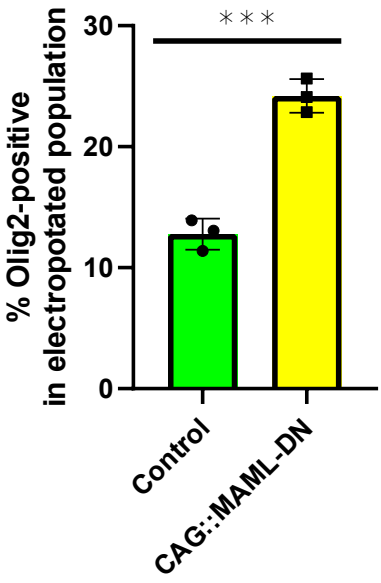
C
% Olig2-positive
in electropotated population
30
20
10
0
***
Control
CAG::MAML-DN

Fig. 4

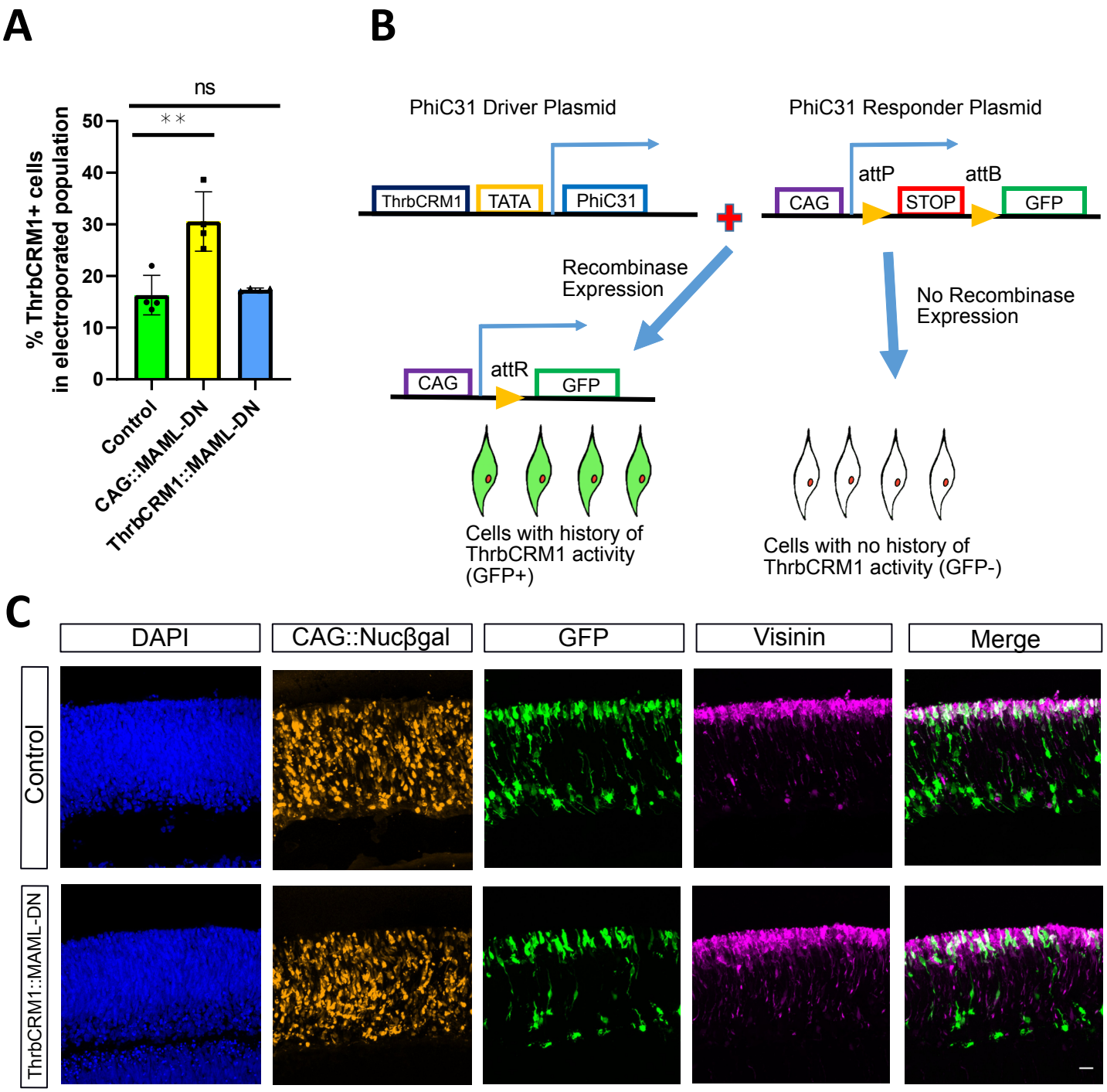
A
ns
**
% ThrbCRM1+ cells in electroporated population
50
40
30
20
10
0
Control
CAG::MAML-DN
ThrbCRM1::MAML-DN
B
PhiC31 Driver Plasmid
ThrbCRM1
TATA
PhiC31
PhiC31 Responder Plasmid
CAG
attP
STOP
attB
GFP
Recombinase Expression
No Recombinase Expression
CAG
attR
GFP
Cells with history of ThrbCRM1 activity (GFP+)
Cells with no history of ThrbCRM1 activity (GFP-)
C
DAPI
CAG::Nucβgal
GFP
Visinin
Merge
Control
ThrbCRM1::MAML-DN

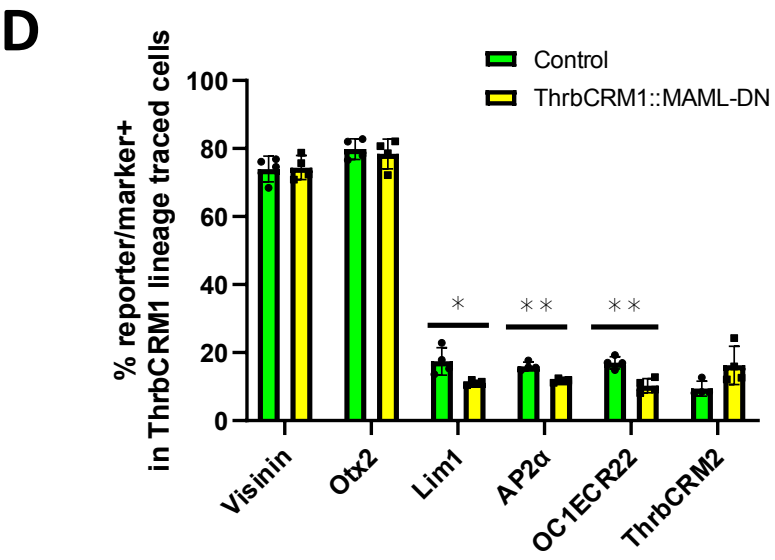
D
Control
ThrbCRM1::MAML-DN
% reporter/marker+ in ThrbCRM1 lineage traced cells
100
80
60
40
20
0
*
**
**
Visinin
Otx2
Lim1
AP2α
OC1ECR22
ThrbCRM2

Fig. 5

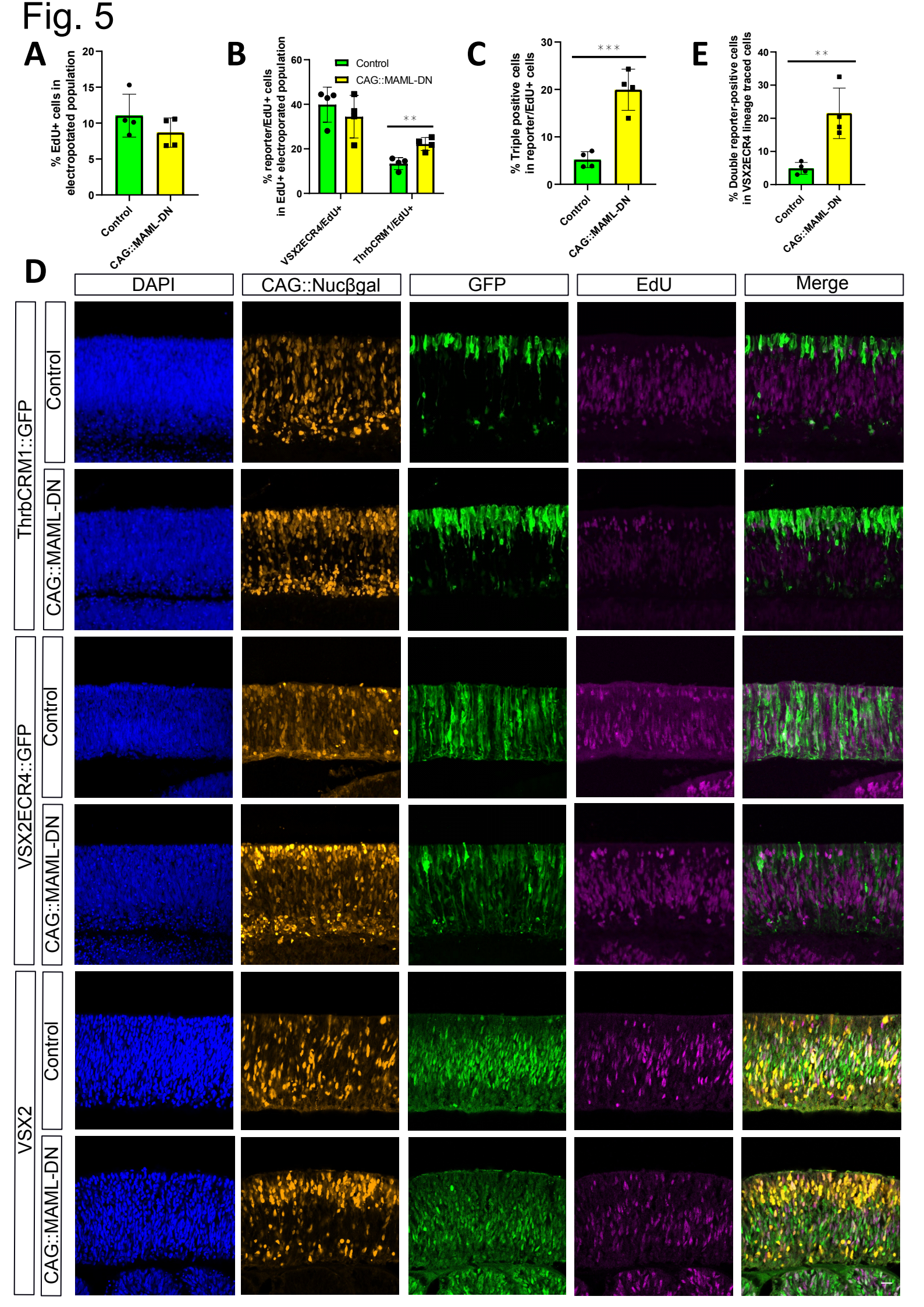
A
% EdU+ cells in electropotated population
20
15
10
5
0
Control
CAG::MAML-DN
B
% reporter/EdU+ cells in EdU+ electroporated population
60
40
20
0
Control
CAG::MAML-DN
**
VSX2ECR4/EdU+
ThrbCRM1/EdU+
C
% Triple positive cells in reporter/EdU+ cells
30
20
10
0
***
Control
CAG::MAML-DN
E
% Double reporter-positive cells in VSX2ECR4 lineage traced cells
40
30
20
10
0
**
Control
CAG::MAML-DN
D
DAPI
CAG::Nucβgal
GFP
EdU
Merge
ThrbCRM1::GFP
Control
CAG::MAML-DN
VSX2ECR4::GFP
Control
CAG::MAML-DN
VSX2
Control
CAG::MAML-DN

Fig. 6

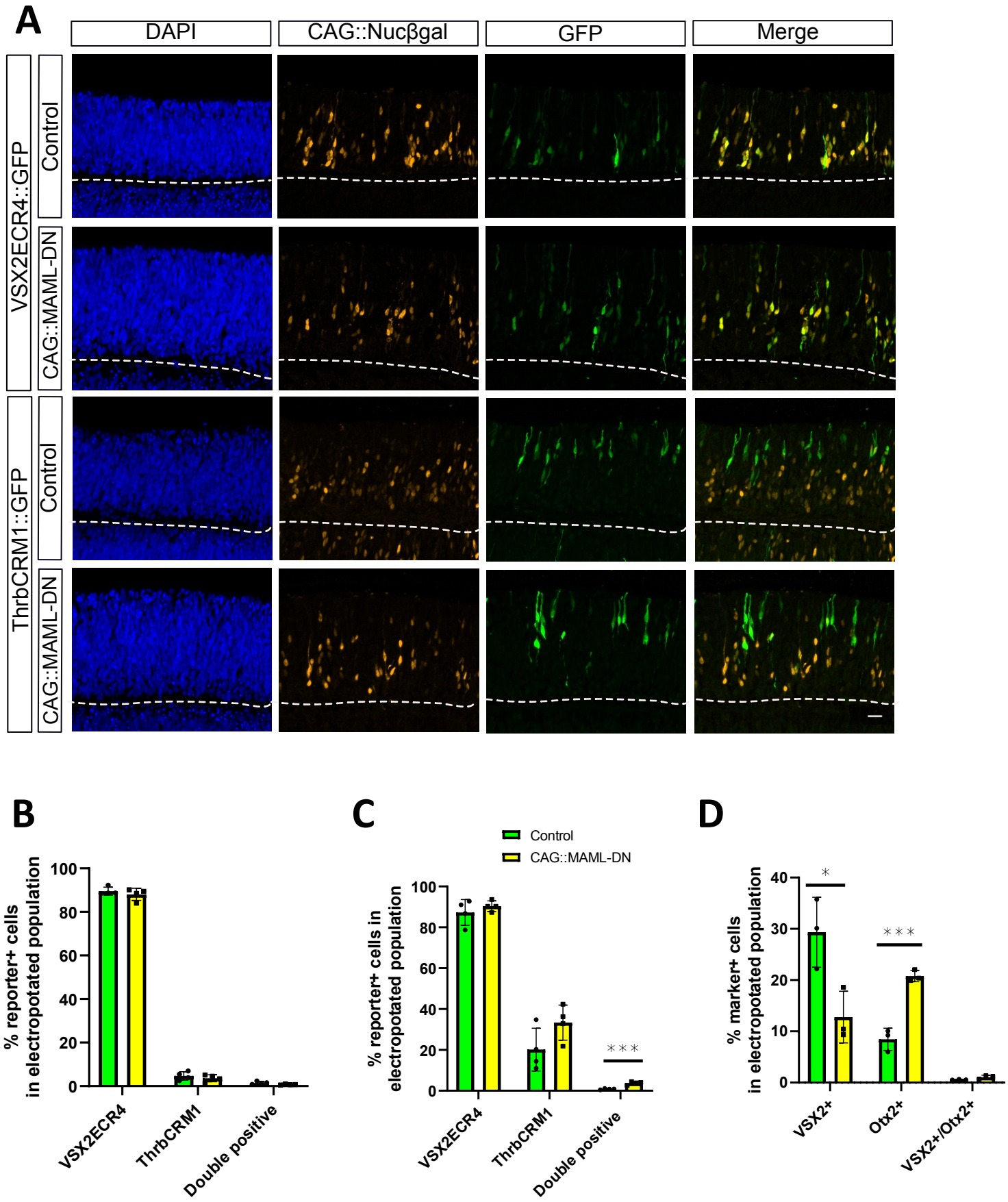
A
DAPI
CAG::Nucβgal
GFP
Merge
VSX2ECR4::GFP
Control
CAG::MAML-DN
ThrbCRM1::GFP
Control
CAG::MAML-DN
B
% reporter+ cells in electropotated population
100
80
60
40
20
0
VSX2ECR4
ThrbCRM1
Double positive
C
Control
CAG::MAML-DN
% reporter+ cells in electropotated population
100
80
60
40
20
0
***
VSX2ECR4
ThrbCRM1
Double positive
D
% marker+ cells in electropotated population
40
30
20
10
0
*
***
VSX2+
Otx2+
VSX2+/Otx2+

Fig. 7

A

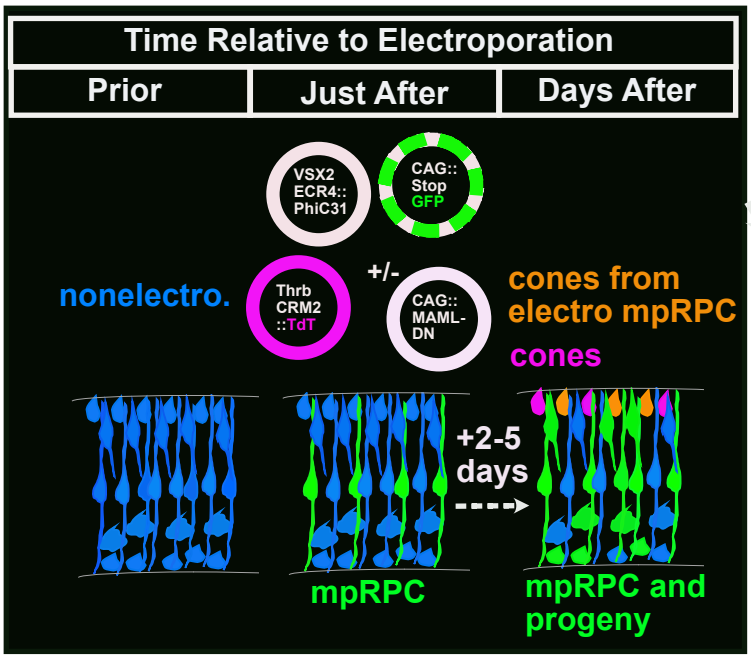
Time Relative to Electroporation
Prior
Just After
Days After
VSX2 ECR4:: PhiC31
CAG:: Stop GFP
nonelectro.
Thrb CRM2 ::TdT
+/-
CAG:: MAML-DN
cones from electro mpRPC
cones
+2-5 days
mpRPC
mpRPC and progeny

B

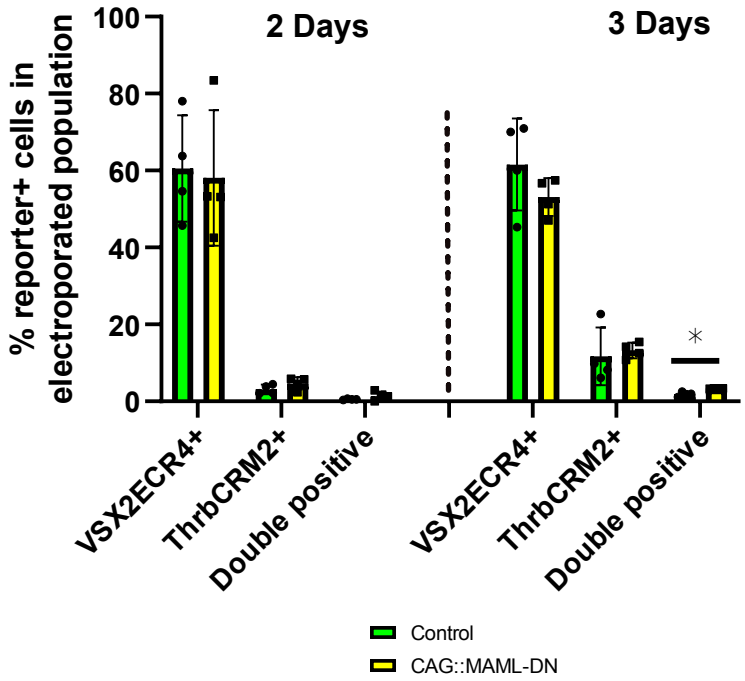
% reporter+ cells in electroporated population
100
80
60
40
20
0
2 Days
3 Days
*
VSX2ECR4+
ThrbCRM2+
Double positive
VSX2ECR4+
ThrbCRM2+
Double positive
Control
CAG::MAML-DN

C

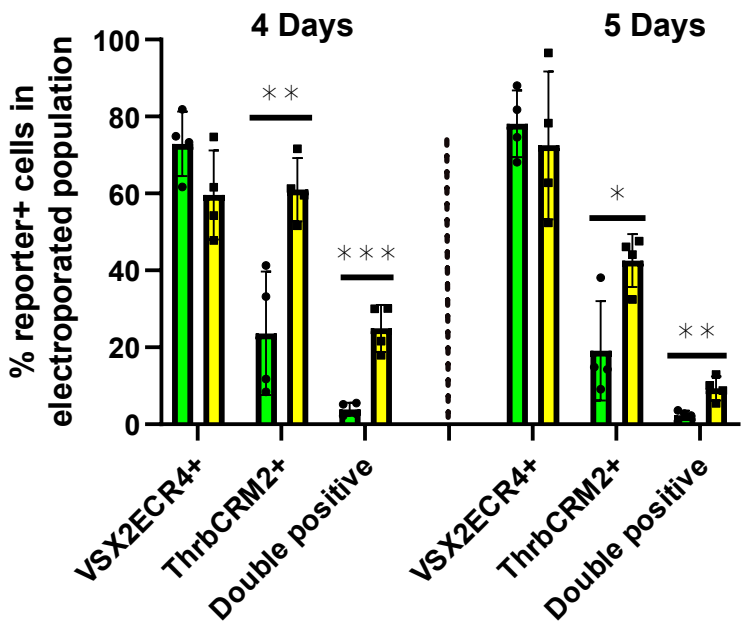
% reporter+ cells in electroporated population
100
80
60
40
20
0
4 Days
5 Days
**
***
*
**
VSX2ECR4+
ThrbCRM2+
Double positive
VSX2ECR4+
ThrbCRM2+
Double positive

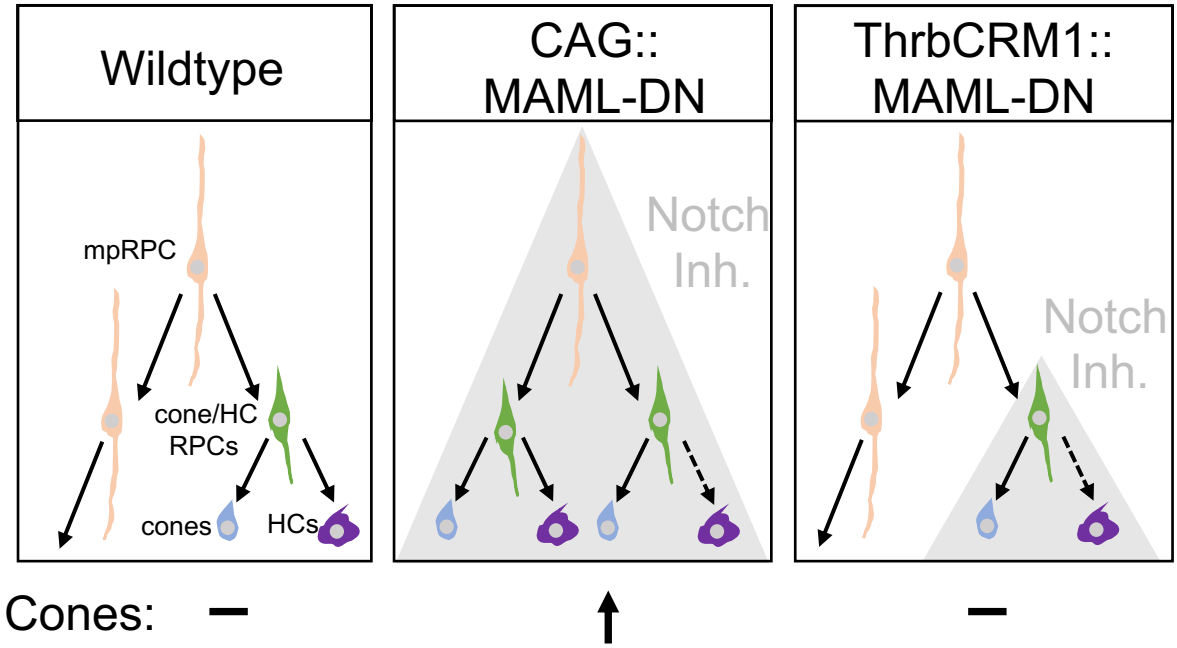
Wildtype
CAG::
MAML-DN
ThrbCRM1::
MAML-DN
mpRPC
cone/HC
RPCs
cones
HCs
Notch
Inh.
Notch
Inh.
Cones:
–
↑
–

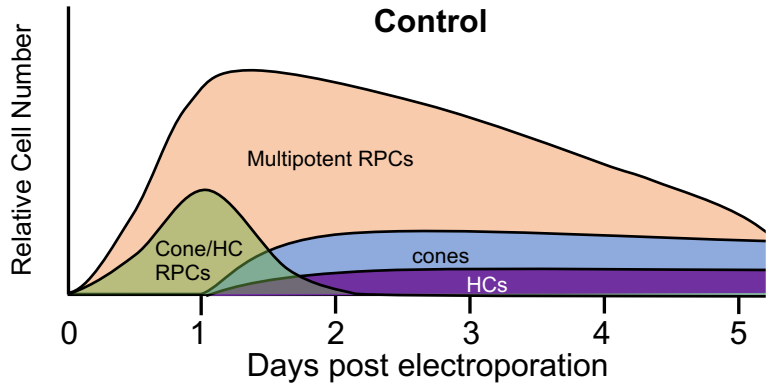
Control
Relative Cell Number
Multipotent RPCs
Cone/HC
RPCs
cones
HCs
0
1
2
3
4
5
Days post electroporation

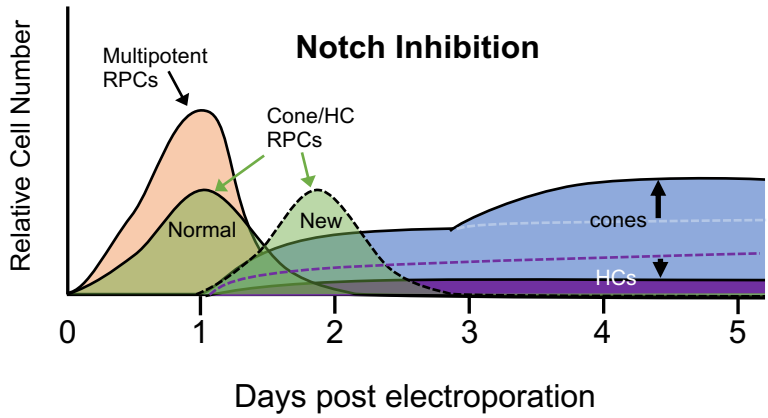
Notch Inhibition
Relative Cell Number
Multipotent
RPCs
Cone/HC
RPCs
Normal
New
cones
HCs
0
1
2
3
4
5
Days post electroporation